As I ebb'd with the ocean of life,
As I wended the shores I know,
As I walk'd where the ripples continually wash you Paumanok …
As the ocean so mysterious rolls toward me closer and closer …
I perceive I have not really understood any thing,
not a single object, and that no man ever can,
Nature here in sight of the sea taking advantage of me
to dart upon me and sting me,
Because I have dared to open my mouth to sing at all.

Walt Whitman, *As I Ebb'd with the Ocean of Life,* from *Leaves of Grass,* 1881.

CHAPTER 19

Wind-Driven Gyres

UNDERSTANDING THE CIRCULATION OF THE OCEAN involves a combination of observations, comprehensive numerical modelling, and more conceptual modelling or theory.[1] All are essential, but in this chapter and the ones following our emphasis is on the last of the triad. Its (continuing) role is not to explain every feature of the observed ocean circulation, nor to necessarily describe details best left to numerical simulations. Rather, it is to provide a conceptual and theoretical framework for understanding the circulation of the ocean, for interpreting observations and suggesting how new observations may best be made, and to aid the development and interpretation of numerical models.

The aspect of the ocean that most affects the climate is the sea-surface temperature (SST), as illustrated in Fig. 19.1, and aside from the expected latitudinal variation there is significant zonal variation too — the western tropical Pacific is particularly warm, and the western Atlantic is warmer than the corresponding latitude in the east. These variations owe their existence to ocean currents, and the main ones are sketched — in a highly schematic and non-quantitative fashion — in Fig. 19.2. Over most of the ocean, the vertically averaged currents have a similar sense to the surface currents, one exception being at the equator where the surface currents are mainly westward but the vertical integral is dominated by the eastward undercurrent. Two dichotomous aspects of this picture stand out: (i) the complexity of the currents as they interact with topography and the geography of the continents; (ii) the simplicity and commonality of the large-scale structures in the major ocean basins, and in particular the ubiquity of subtropical and subpolar gyres. Indeed these gyres, sweeping across the great oceans carrying vast quantities of water and heat, are perhaps the single most conspicuous feature of the circulation. The subtropical gyres are anticyclonic, extending polewards to about 45°, and the subpolar gyres are cyclonic and polewards of this, primarily in the Northern Hemisphere. The existence of the great gyres, and that they are strongest in the west, has been known for centuries; this *western intensification* leads to such well-known currents as the Gulf Stream in the Atlantic (charted by Benjamin Franklin), the Kuroshio in the Pacific, and the Brazil Current in the South Atlantic.

For much of this chapter we consider a model, and variations about it, that explains the large-scale features of ocean gyres and that lies at the core of ocean circulation theory — the steady, forced-dissipative, homogeneous model of the ocean circulation first formulated by Stommel.[2] In all of the geosciences there is perhaps no other model that combines elegance and as relevance as much as this one.

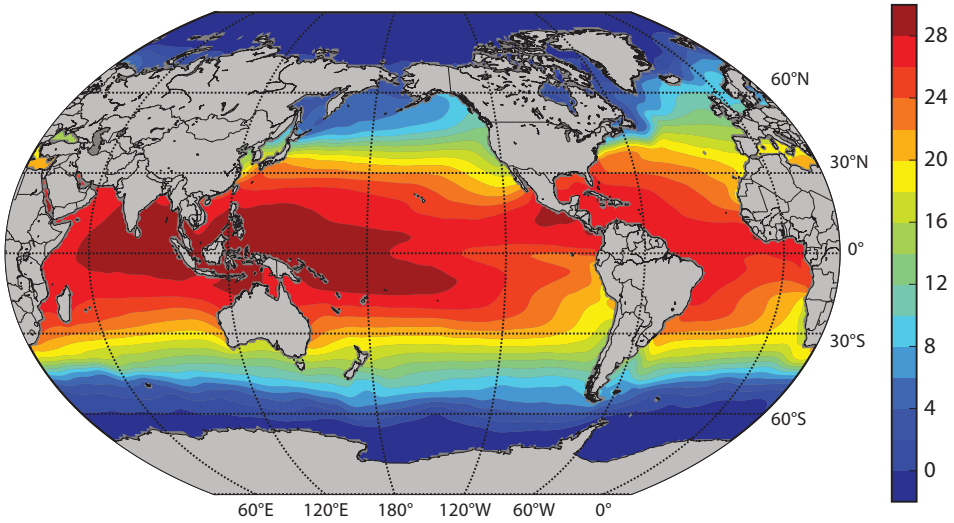

Fig. 19.1 The sea-surface temperature (SST, ° C) of the world's ocean, as determined from a great many observations, combined in the World Ocean Circulation Experiment (WOCE).

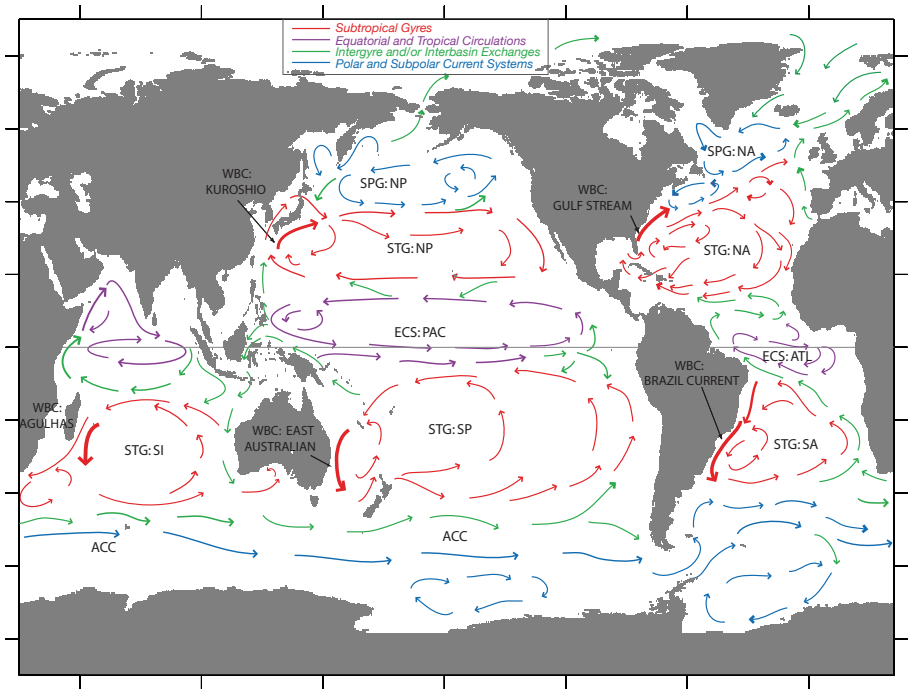

Fig. 19.2 Idealization of the main currents of the global ocean. Key: STG – Subtropical Gyre; SPG – Subpolar Gyre; WBC – Western Boundary Current; ECS – Equatorial Current System; NA – North Atlantic; SA – South Atlantic; NP – North Pacific; SP – South Pacific; SI – South Indian; ACC – Antarctic Circumpolar Current; ATL – Atlantic; PAC – Pacific. The figure is only a qualitative representation of the actual flow. Most of the currents are manifested at the surface, but near the equator the figure shows the undercurrent which flows in the opposite way to the surface current.

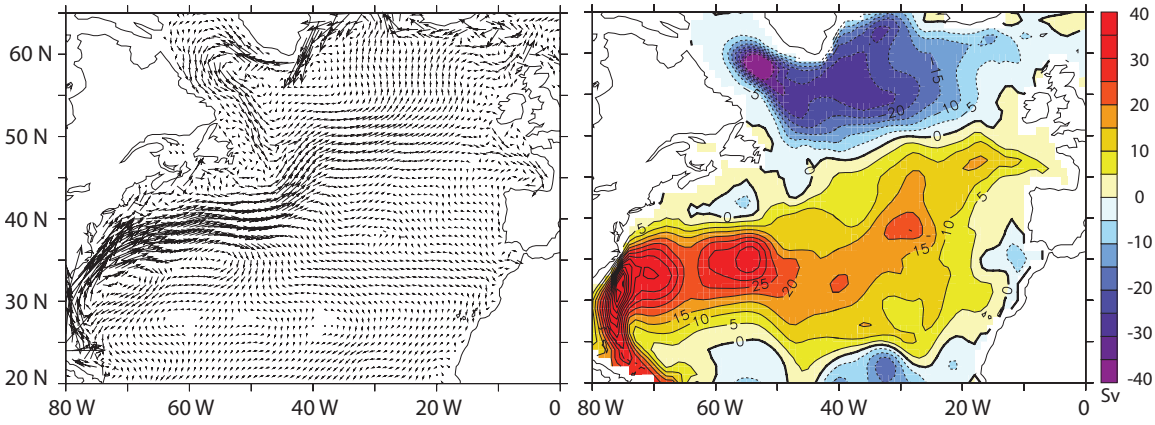

Fig. 19.3 Left: the time averaged velocity field at a depth of 75 m in the North Atlantic, obtained by constraining a numerical model to observations (so giving a 'state estimate'). Right: the streamfunction of the vertically integrated flow, in Sverdrups ($1\,\mathrm{Sv} = 10^9\,\mathrm{kg\,s^{-1}}$). Note the presence of an anticyclonic subtropical gyre (clockwise circulation, shaded red), a cyclonic subpolar gyre (anticlockwise, blue), and intense western boundary currents.[4]

19.1 THE DEPTH INTEGRATED WIND-DRIVEN CIRCULATION

Although even today we barely have sufficient observations to produce a detailed synoptic map of the ocean currents, except at the surface, the large-scale mean currents are fairly well mapped and Fig. 19.3 illustrates the average current pattern of the North Atlantic using a combination of observations and a numerical model, and the Gulf Stream is clearly visible. Similar features are seen in all the major ocean basins (Fig. 19.4) where we see subtropical and subpolar gyres, all of them intensified in the west.[3] Our goal in this chapter is to explain the main features seen in these figures in as simple and straightforward a manner as is possible.

The equations that govern the large-scale flow in the oceans are the planetary-geostrophic equations. Greatly simplified as these are compared to the Navier–Stokes equations, or even the hydrostatic Boussinesq equations, they are still quite daunting: a prognostic equation for buoyancy is coupled to the advecting velocity via hydrostatic and geostrophic balance, and the resulting problem is formidably nonlinear. However, it turns out that thermodynamic effects can effectively be eliminated by the simple device of vertical integration; the resulting equations are linear, and the only external forcing is that due to the wind stress. The resulting model then, at the price of some comprehensiveness, gives a useful picture of the *wind-driven* circulation of the ocean. We will consider the vertical structure of this flow in the next chapter.

19.1.1 The Stommel Model

The planetary-geostrophic equations for a Boussinesq fluid are:

$$\frac{\mathrm{D}b}{\mathrm{D}t} = \dot{b}, \qquad \nabla_3 \cdot \boldsymbol{v} = 0, \tag{19.1a,b}$$

$$\boldsymbol{f} \times \boldsymbol{u} = -\nabla\phi + \frac{1}{\rho_0}\frac{\partial \boldsymbol{\tau}}{\partial z}, \qquad \frac{\partial \phi}{\partial z} = b. \tag{19.2a,b}$$

These equations are, respectively, the thermodynamic equation (19.1a), the mass continuity equation (19.1b), the horizontal momentum equation (19.2a), (i.e., geostrophic balance, plus a stress

term), and the vertical momentum equation (19.2b) — that is, hydrostatic balance. These equations are derived more fully in Chapter 5, but they are essentially the Boussinesq primitive equations with the advection terms omitted from the horizontal momentum equation, on the basis of small Rossby number. In this chapter we will henceforth absorb the factor of ρ_0 into the $\boldsymbol{\tau}$, so that $\boldsymbol{\tau}$ denotes the kinematic stress, and the gradient operator will be two dimensional, in the x-y plane, unless noted.

Take the curl of (19.2a) (that is, cross differentiate its x and y components) and integrate over the depth of the ocean to give

$$\int f \nabla \cdot \boldsymbol{u} \, \mathrm{d}z + \frac{\partial f}{\partial y} \int v \, \mathrm{d}z = \mathrm{curl}_z(\boldsymbol{\tau}_T - \boldsymbol{\tau}_B), \tag{19.3}$$

where the operator curl_z is defined by $\mathrm{curl}_z \boldsymbol{A} \equiv \partial A^y/\partial x - \partial A^x/\partial y = \mathbf{k} \cdot \nabla \times \boldsymbol{A}$, and the subscripts T and B are for top and bottom. The divergence term vanishes if the vertical velocity is zero at the top and bottom of the ocean. Strictly, at the top of the ocean the vertical velocity is given by the material derivative of height of the ocean's surface, $\mathrm{D}h/\mathrm{D}t$, but on the large-scales this has a negligible effect and we may make the rigid-lid approximation and set it to zero. At the bottom of the ocean the vertical velocity is only zero if the ocean is flat-bottomed; otherwise it is $\boldsymbol{u} \cdot \nabla \eta_B$, where η_B is the orographic height at the ocean floor. The neglect of this topographic term is probably the most restrictive single approximation in the model. Given this neglect, (19.3) becomes

$$\beta \overline{v} = \mathrm{curl}_z(\boldsymbol{\tau}_T - \boldsymbol{\tau}_B), \tag{19.4}$$

where henceforth, in this section, quantities with an overbar are understood to be the vertical integral over the depth of the ocean. If the stresses depend only on the velocity fields then thermodynamic fields do not affect the vertically integrated flow.

At the top of the ocean, the stress is given by the wind. At the bottom, in the absence of topography we assume that the stress may be parameterized by a linear drag, or Rayleigh friction, as might be generated by an Ekman layer; it is this assumption that particularly characterizes this model as being due to Stommel. (Note that we parameterize the friction by a drag acting on the vertically integrated velocity. Using the velocity at the bottom of the ocean would be more realistic, but this wrinkle is beyond the scope of vertically integrated models.) Equation (19.4) then becomes

$$\beta \overline{v} = -r\overline{\zeta} + F_\tau(x, y), \tag{19.5}$$

where $F_\tau = \mathrm{curl}_z \boldsymbol{\tau}_T$ is the wind-stress curl at the top of the ocean and is a known function. Because the velocity is divergence-free, we can define a streamfunction ψ such that $\overline{u} = -\partial\psi/\partial y$ and $\overline{v} = \partial\psi/\partial x$. Equation (19.5) then becomes

$$r\nabla^2\psi + \beta\frac{\partial \psi}{\partial x} = F_\tau(x, y). \tag{19.6}$$

This equation is often referred to as the *Stommel problem* or the *Stommel model,* and may be posed in a variety of two dimensional domains.

19.1.2 Alternative Formulations

A number of alternative formulations leading to (19.6) are possible. None are perhaps as well justified as the derivation via the planetary-geostrophic equations but the differences in the specific assumptions made give some indication of the robustness of the derivation, and show how the model might be extended to include topographic or nonlinear effects.

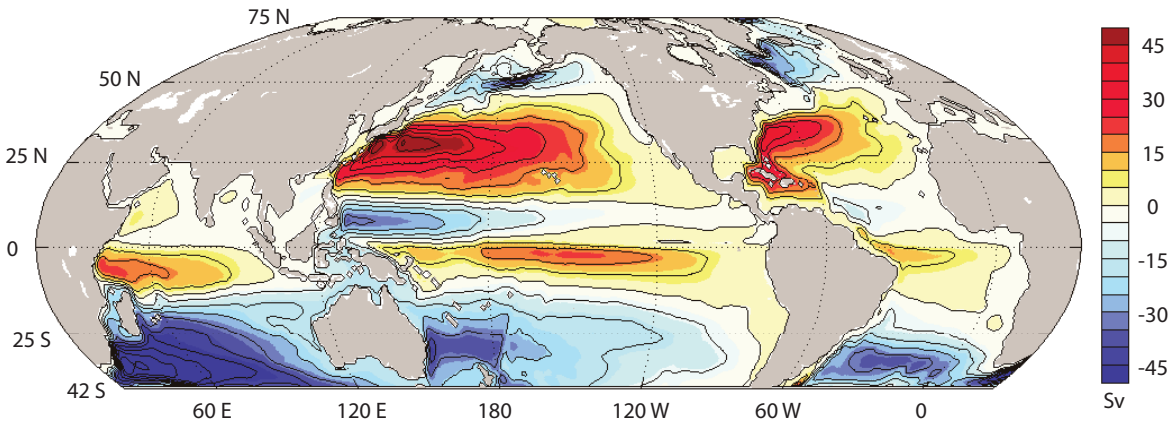

Fig. 19.4 A state estimate of the streamfunction of the vertically integrated flow for the near global ocean. Red shading indicates clockwise flow, and blue shading anticlockwise, but in both hemispheres the subtropical (subpolar) gyres are anticyclonic (cyclonic).[5]

I. A homogeneous model

Rather than vertically integrating, we may suppose that the ocean is a homogeneous fluid obeying the shallow water equations (Chapter 3). The potential vorticity equation (cf. (3.96) on page 121) is:

$$\frac{\mathrm{D}}{\mathrm{D}t}\left(\frac{\zeta + f}{h}\right) = \frac{F}{h}, \tag{19.7}$$

where F represents friction and forcing. In an ocean with a rigid-lid and flat bottom (19.7) gives the barotropic vorticity equation,

$$\frac{\mathrm{D}\zeta}{\mathrm{D}t} + \beta v = F, \tag{19.8}$$

where the term F again represents the wind-stress curl and a linear drag. Further, since the horizontal velocity is divergence-free (because of the flat-bottom and rigid-lid) we may represent it as a streamfunction, whence we obtain the closed equation

$$\frac{\mathrm{D}}{\mathrm{D}t}\nabla^2\psi + \beta\frac{\partial\psi}{\partial x} = F_\tau(x, y) - r\nabla^2\psi, \tag{19.9}$$

where F_τ again represents the wind forcing. This equation is the 'time-dependent nonlinear Stommel problem'. The steady nonlinear problem is sometimes of interest, too, and this is just

$$J(\psi, \nabla^2\psi) + \beta\frac{\partial\psi}{\partial x} = F_\tau(x, y) - r\nabla^2\psi. \tag{19.10}$$

To obtain the original Stommel model we just ignore the advective derivative, which will be valid if $|\zeta| \sim Z \ll \beta L$ where $Z = U/L$ is a representative value of vorticity. This condition is equivalent to

$$R_\beta \equiv \frac{U}{\beta L^2} \ll 1. \tag{19.11}$$

R_β is called the *beta-Rossby number.* On sufficiently large scales, $\beta \sim f/L$ and (19.11) is similar to a small Rossby number assumption.

II. Quasi-geostrophic formulation

In the planetary-geostrophic formulation, the horizontal velocity is divergence-free only because we have vertically integrated. If the scales of motion are not too large the horizontal flow at every level is divergence-free for another reason: because it is in geostrophic balance. In reality, over a single oceanic gyre (say from 15° to 40° latitude), variations in Coriolis parameter are not large, and this prompts us to formulate the model in terms of the quasi-geostrophic equations. Formally, such a model would then be restricted to length scales, L, of no more than $\mathcal{O}(Ro^{-1})$ larger than the deformation radius, and for gyre scales this criterion is marginally satisfied if $L_d = 100\,\text{km}$. An advantage of the quasi-geostrophic equations is that they readily allow for the inclusion of both nonlinearity and stratification. (For an informal summary of quasi-geostrophy, see the box on page 193.) The quasi-geostrophic vorticity equation for a Boussinesq system is:

$$\frac{\mathrm{D}\zeta}{\mathrm{D}t} + \beta v = f_0 \frac{\partial w}{\partial z} + \mathrm{curl}_z \frac{\partial \boldsymbol{\tau}}{\partial z}. \tag{19.12}$$

If we neglect the advective derivative, and vertically integrate, we obtain

$$\beta \int_B^T v \, \mathrm{d}z = f_0 [w]_B^T + \mathrm{curl}_z [\boldsymbol{\tau}]_B^T. \tag{19.13}$$

where T denotes the ocean top and B the bottom. We now make one of two virtually equivalent choices:

(i) We suppose that the integration is over the entire depth of the ocean, in which case the term $[w]_B^T$ vanishes given a rigid lid and a flat bottom. If the stress at the top of the ocean is given by the wind stress, and at the bottom of the ocean it is parameterized by a linear drag, then we obtain

$$\beta \overline{v} = F_\tau(x, y) - r\overline{\zeta} \tag{19.14}$$

just as in (19.5), and where an overbar denotes a vertical integral. Writing $\overline{v} = \partial\psi/\partial x$ and $\overline{\zeta} = \nabla^2\psi$ then gives (19.6).

(ii) We suppose that the integration is between two thin Ekman layers at the top and bottom of the ocean. The stress is zero at the interior edge of these layers, but the vertical velocity is not. At the base of the upper Ekman layer, at $z = -\delta_T$, the vertical velocity is given by:

$$w(x, y, -\delta_T) = \mathrm{curl}_z(\boldsymbol{\tau}_T / f_0), \tag{19.15}$$

where the top of the ocean is at $z = 0$ and δ_T is the thickness of the upper Ekman layer. Similarly, at the top of the lower Ekman layer, the vertical velocity is:

$$w(x, y, -H + \delta_B) = \delta_B \zeta, \tag{19.16}$$

where $z = -H$ at the ocean bottom and δ_B is the thickness of the bottom Ekman layer. Neglecting the advective derivative, and integrating over the ocean between the two Ekman layers, (19.12) becomes

$$\beta \overline{v} = \mathrm{curl}_z \boldsymbol{\tau}_T - f_0 \delta_B \zeta = \mathrm{curl}_z \boldsymbol{\tau}_T - f_0 \delta_B \overline{\zeta}/H, \tag{19.17}$$

where, to obtain the second equality, we assume that the bottom drag may be parameterized using the vertically integrated vorticity, $\overline{\zeta}$. Defining the drag coefficient r by $r = f_0\delta_B/H$, and introducing a streamfunction gives

$$r\nabla^2\psi + \beta \frac{\partial \psi}{\partial x} = \mathrm{curl}_z \boldsymbol{\tau}_T, \tag{19.18}$$

as before.

19.1.3 Approximate Solution of Stommel Model

Sverdrup balance

Equation (19.6) is linear and it is possible to obtain an exact, analytic solution. However, it is more insightful to approach the problem perturbatively, by supposing that the frictional term is small, meaning there is an approximate balance between wind stress and the β-effect.[6] Friction is small if $|r\zeta| \ll |\beta v|$ or

$$\frac{r}{L} = \frac{f\delta_B}{HL} \ll \beta \tag{19.19}$$

using $r = f\delta_B/H$, and where L is the horizontal scale of the motion, and generally speaking this inequality is well satisfied for large-scale flow. The vorticity equation becomes

$$\beta\overline{v} \approx \mathrm{curl}_z \boldsymbol{\tau}_T, \tag{19.20}$$

which is known as *Sverdrup balance*.[7] (Sometimes Sverdrup balance is taken to mean the linear geostrophic vorticity balance $\beta v = f\partial w/\partial z$, but we will restrict its use to mean a balance between the beta effect and wind stress curl.) The observational support for Sverdrup balance is rather mixed, discrepancies arising not so much from the failure of (19.19), but from the presence of small-scale eddying motion with concomitantly large nonlinear terms, and the presence of non-negligible vertical velocities induced by the interaction with bottom topography.[8] Nevertheless, Sverdrup balance provides a useful, if not impregnable, foundation on which to build.

Boundary-layer solution

For simplicity, consider a square domain of side a and rescale the variables by setting

$$x = a\hat{x}, \qquad y = a\hat{y}, \qquad \tau = \tau_0\hat{\tau}, \qquad \psi = \hat{\psi}\frac{\tau_0}{\beta}, \tag{19.21}$$

where τ_0 is the amplitude of the wind stress. The hatted variables are nondimensional and, assuming our scaling to be sensible, these are $\mathcal{O}(1)$ quantities in the interior. Equation (19.18) becomes

$$\frac{\partial\hat{\psi}}{\partial\hat{x}} + \epsilon_S\nabla^2\hat{\psi} = \mathrm{curl}_z\hat{\boldsymbol{\tau}}_T, \tag{19.22}$$

where $\epsilon_S = (r/a\beta) \ll 1$, in accord with (19.19). For the rest of this section we will drop the hats over nondimensional quantities. Over the interior of the domain, away from boundaries, the frictional term in (19.22) is small. We can take advantage of this by writing

$$\psi(x, y) = \psi_I(x, y) + \phi(x, y), \tag{19.23}$$

where ψ_I is the interior streamfunction and ϕ is a boundary layer correction. Away from boundaries ψ_I is presumed to dominate the flow, and this satisfies

$$\frac{\partial\psi_I}{\partial x} = \mathrm{curl}_z\boldsymbol{\tau}_T. \tag{19.24}$$

The solution of this equation (called the 'Sverdrup interior') is

$$\psi_I(x, y) = \int_0^x \mathrm{curl}_z\boldsymbol{\tau}(x', y)\,\mathrm{d}x' + g(y), \tag{19.25}$$

where $g(y)$ is an arbitrary function of integration that gives rise to an arbitrary zonal flow. The corresponding velocities are

$$v_I = \mathrm{curl}_z\boldsymbol{\tau}, \qquad u_I = -\frac{\partial}{\partial y}\int_0^x \mathrm{curl}_z\boldsymbol{\tau}(x', y)\,\mathrm{d}x' - \frac{\mathrm{d}g(y)}{\mathrm{d}y}. \tag{19.26}$$

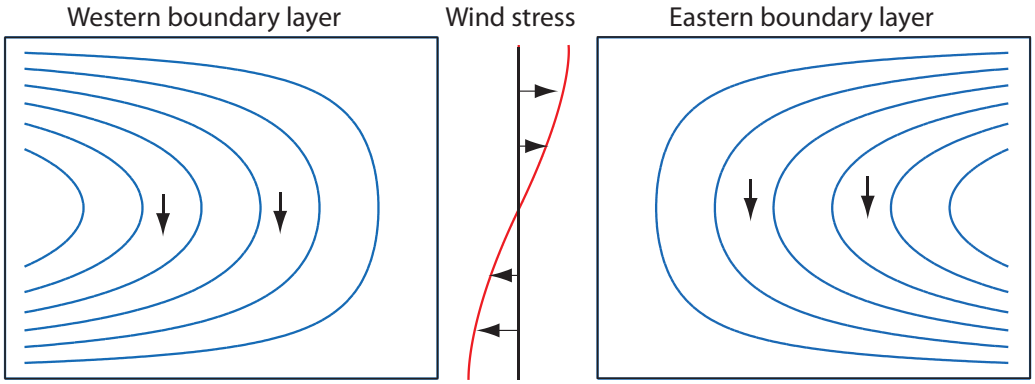

Fig. 19.5 Two possible Sverdrup flows, ψ_I, for the wind stress shown in the centre. Each solution satisfies the no-flow condition at either the eastern or western boundary, and a boundary layer is therefore required at the other boundary. Both flows have the same, equatorward, meridional flow in the interior. Only the flow with the western boundary current is physically realizable, however, because only then can friction produce a curl that opposes that of the wind stress, so allowing the flow to equilibrate.

The dynamics is most clearly illustrated if we now restrict our attention to a wind-stress curl that is zonally uniform, and that vanishes at two latitudes, $y = 0$ and $y = 1$. An example is

$$\tau_T^y = 0, \qquad \tau_T^x = -\cos(\pi y), \tag{19.27}$$

for which $\mathrm{curl}_z \boldsymbol{\tau}_T = -\pi \sin(\pi y)$. The Sverdrup (interior) flow may then be written as

$$\psi_I(x, y) = [x - C(y)]\mathrm{curl}_z \boldsymbol{\tau}_T = \pi[C(y) - x] \sin \pi y, \tag{19.28}$$

where $C(y)$ is the arbitrary function of integration $[C(y) = -g(y)/\mathrm{curl}_z \boldsymbol{\tau}]$. If we choose C to be a constant, the zonal flow associated with it is $C\,\mathrm{curl}_z \boldsymbol{\tau}_T$. We can then satisfy $\psi = 0$ at *either* $x = 0$ (if $C = 0$) *or* $x = 1$ (if $C = 1$). These solutions are illustrated in Fig. 19.5 for the particular stress (19.27).

Regardless of our choice of C we cannot satisfy $\psi = 0$ at both zonal boundaries. We must choose one, and then construct a *boundary layer* solution (i.e., we determine ϕ) to satisfy the other condition. Which choice do we make? On intuitive grounds it seems that we should choose the solution that satisfies $\psi = 0$ at $x = 1$ (the solution on the left in Fig. 19.5), for the interior flow then goes round in the same direction as the wind: the wind is supplying a clockwise torque, and to achieve an angular momentum balance anticlockwise angular momentum must be supplied by friction. We can imagine that this would be provided by the frictional forces at the western boundary layer if the interior flow is clockwise, but not by friction at an eastern boundary layer when the interior flow is anticlockwise. Note that this argument is not dependent on the sign of the wind-stress curl: if the wind blew the other way a similar argument still implies that a western boundary layer is needed. We will now see if and how the mathematics reflects this intuitive but non-rigorous argument.

Asymptotic matching

Near the walls of the domain the boundary layer correction $\phi(x, y)$ must become important in order that the boundary conditions may be satisfied, and the flow, and in particular $\phi(x, y)$, will vary rapidly with x. To reflect this, let us *stretch* the x-coordinate near this point of failure (i.e., at

either $x = 0$ or $x = 1$, but we do not know at which yet) and let

$$x = \epsilon\alpha \qquad \text{or} \qquad x - 1 = \epsilon\alpha. \tag{19.29a,b}$$

Here, α is the stretched coordinate, which has values $\mathcal{O}(1)$ in the boundary layer, and ϵ is a small parameter, as yet undetermined. We then suppose that $\phi = \phi(\alpha, y)$, and using (19.23) in (19.22), we obtain

$$\epsilon_S(\nabla^2\psi_I + \nabla^2\phi) + \frac{\partial\psi_I}{\partial x} + \frac{1}{\epsilon}\frac{\partial\phi}{\partial\alpha} = \text{curl}_z\boldsymbol{\tau}_T, \tag{19.30}$$

where $\phi = \phi(\alpha, y)$ and $\nabla^2\phi = \epsilon^{-2}\partial^2\phi/\partial\alpha^2 + \partial^2\phi/\partial y^2$. Now, by choice, ψ_I exactly satisfies Sverdrup balance, and so (19.30) becomes

$$\epsilon_S\left(\nabla^2\psi_I + \frac{1}{\epsilon^2}\frac{\partial^2\phi}{\partial\alpha^2} + \frac{\partial^2\phi}{\partial y^2}\right) + \frac{1}{\epsilon}\frac{\partial\phi}{\partial\alpha} = 0. \tag{19.31}$$

We now choose ϵ to obtain a physically meaningful solution. An obvious choice is $\epsilon = \epsilon_S$, for then the leading-order balance in (19.31) is

$$\frac{\partial^2\phi}{\partial\alpha^2} + \frac{\partial\phi}{\partial\alpha} = 0, \tag{19.32}$$

the solution of which is

$$\phi = A(y) + B(y)\mathrm{e}^{-\alpha}. \tag{19.33}$$

Evidently, ϕ grows exponentially in the negative α direction. If this were allowed, it would violate our assumption that solutions are small in the interior, and we must eliminate this possibility by allowing α to take only positive values in the interior of the domain, and by setting $A(y) = 0$. We therefore choose $x = \epsilon\alpha$ so that $\alpha > 0$ for $x > 0$; the boundary layer is then at $x = 0$, that is, it is a *western boundary,* and it decays eastwards in the direction of increasing α — that is, into the ocean interior. We now choose $C = 1$ in (19.28) to make $\psi_I = 0$ at $x = 1$ in (19.28) and then, for the wind stress (19.27), the interior solution is given by

$$\psi_I = \pi(1 - x)\sin\pi y. \tag{19.34}$$

This alone satisfies the boundary condition at the eastern boundary. The function $B(y)$ is chosen to satisfy the additional condition that

$$\psi = \psi_I + \phi = 0 \qquad \text{at} \quad x = 0, \tag{19.35}$$

and using (19.34) this gives

$$\pi\sin\pi y + B(y) = 0. \tag{19.36}$$

Using this in (19.33), with $A(y) = 0$, then gives the boundary layer solution

$$\phi = -\pi\sin\pi y\,\mathrm{e}^{-x/\epsilon_S}. \tag{19.37}$$

The composite (boundary layer plus interior) solution is the sum of (19.34) and (19.37), namely

$$\psi = (1 - x - \mathrm{e}^{-x/\epsilon_S})\pi\sin\pi y. \tag{19.38}$$

With dimensional variables this is

$$\psi = \frac{\tau_0\pi}{\beta}\left(1 - \frac{x}{a} - \mathrm{e}^{-x/(a\epsilon_S)}\right)\sin\frac{\pi y}{a}. \tag{19.39}$$

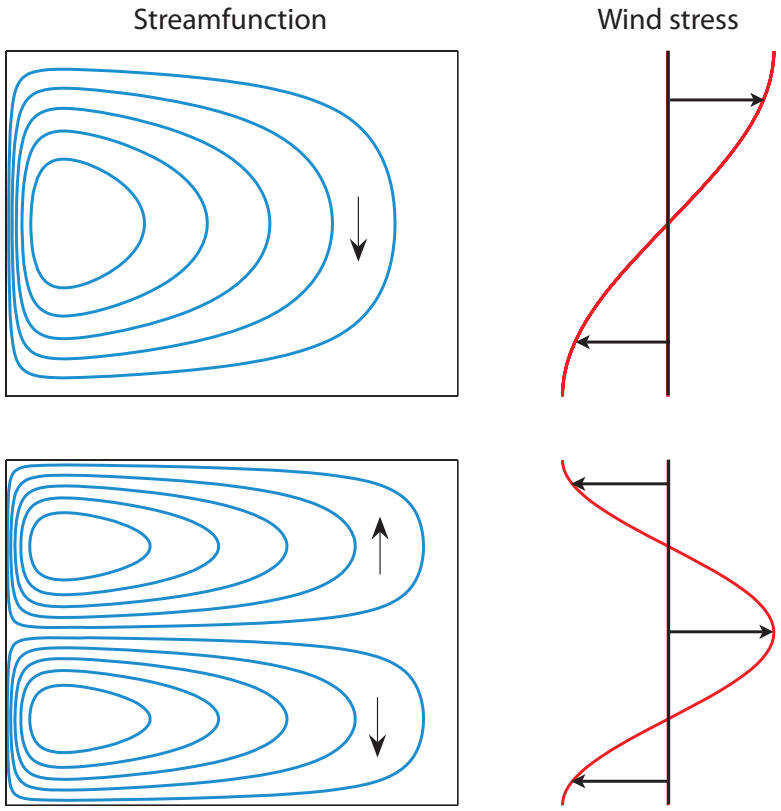

Fig. 19.6 Two solutions of the Stommel model. Upper panel shows the streamfunction of a single-gyre solution, with a wind stress proportional to $-\cos(\pi y/a)$ (in a domain of side a), and the lower panel shows a two-gyre solution, with wind stress proportional to $\cos(2\pi y/a)$. In both cases $\epsilon_S = 0.04$.

This is a 'single gyre' solution. Two or more gyres can be obtained with a different wind forcing, such as $\tau^x = -\tau_0 \cos(2\pi y)$, as in Fig. 19.6.

It is a relatively straightforward matter to generalize to other wind stresses, provided these also vanish at the two latitudes between which the solution is desired. It is left as a problem to show that in general

$$\psi_I = \int_{x_E}^{x} \mathrm{curl}_z \boldsymbol{\tau}(x', y)\, \mathrm{d}x', \tag{19.40}$$

and that the composite solution is

$$\psi = \psi_I - \psi_I(0, y)\mathrm{e}^{-x/(x_E \epsilon_S)}. \tag{19.41}$$

19.2 USING VISCOSITY INSTEAD OF DRAG

A natural variation on the Stommel problem is to use a harmonic viscosity, $\nu\nabla^2\zeta$, in place of the drag term $-r\zeta$ in the vorticity equation, the argument being that the wind-driven circulation does not reach all the way to the ocean bottom so that an Ekman drag is not appropriate. This variation is called the 'Munk problem' or 'Munk model',[9] and if both drag and viscosity are present we have the 'Stommel–Munk' model. The particular form of the lateral friction used in the Munk problem is still somewhat hard to justify because it relies on an ill-founded eddy diffusion of relative vorticity (Chapter 13). Our treatment is brief, focusing on aspects that differ from the Stommel problem. The problem is to find and understand the solution to the (dimensional) equation

$$\beta\frac{\partial\psi}{\partial x} = \mathrm{curl}_z \boldsymbol{\tau}_T + \nu\nabla^2\zeta = \mathrm{curl}_z \boldsymbol{\tau}_T + \nu\nabla^4\psi \tag{19.42}$$

The Stommel and Munk models of the Wind-Driven Circulation

Formulation

- Vertically integrated planetary-geostrophic equations, or a homogeneous fluid with nonlinearity neglected.
- Friction parameterized by a linear drag (Stommel model) or a harmonic Newtonian viscosity (Munk model) or both (Stommel–Munk model).
- Flat bottomed ocean.

Variations on the theme include allowing nonlinearity in the vorticity equation, posing the problem in domains of various shapes, and allowing bottom topography (in particular sloping sidewalls). The solutions are most usefully calculated in the boundary-layer approximation, but some exact solutions exist.

Properties

- The transport in the Sverdrup interior is equatorwards for an anti-cyclonic wind-stress curl. This transport is exactly balanced by the poleward transport in the western boundary layer.
- There must be a boundary layer to satisfy mass conservation, and this must be a *western* boundary layer if the friction acts to provide a force of opposite sign to the motion itself. As there is a balance between friction and the β-effect, it is a 'frictional boundary layer'. The western location does not depend on the sign of the wind stress, nor on the sign of the Coriolis parameter, but it does depend on the sign of β, and so on the direction of rotation of the Earth.
- In the Stommel model the boundary layer width arises by noting that the terms $r\nabla^2\psi$ and $\beta\partial\psi/\partial x$ are in approximate balance in the western boundary layer, implying boundary-layer scale of $L_S = (r/\beta)$. If r, the inverse frictional time, is chosen to be $1/20\,\text{days}^{-1}$ then $L_S \approx 60\,\text{km}$, similar to the width of the Gulf Stream. Unless the wind has a special form the Sverdrup flow is non-zero on the zonal walls and there must also be boundary layers there, but they are weaker and less visible.
- In the Munk model the balance in western boundary layer is between $\nu\nabla^4\psi$ and $\beta\partial\psi/\partial x$, implying a scale of $L_M = (\nu/\beta)^{1/3}$. There are also weak boundary layers on the eastern and zonal walls, to satisfy the no-slip (or free slip) condition.

in a given domain, for example a square of side a. We need two boundary conditions at each wall to solve the problem uniquely, and as before for one of them we choose $\psi = 0$ to satisfy the no-normal-flow condition. For the other condition, two possibilities present themselves:

(i) Zero vorticity, or $\zeta = 0$. Since $\psi = 0$ along the boundary, this possibility is equivalent to $\partial^2\psi/\partial n^2 = 0$ where $\partial/\partial n$ denotes a derivative normal to the boundary. This is known as the 'free-slip' condition. At $x = 0$, for example, the condition becomes $\partial v/\partial x = 0$; that is, there is no horizontal shear at the boundary.

(ii) No flow along the boundary (the no-slip condition). That is $\psi_n = 0$ where the subscript denotes the normal derivative of the streamfunction. At $x = 0$ we have $v = 0$.

There is little a-priori justification for choosing either of these. The second choice would be de-

manded if ν were a molecular viscosity, but then we would have to resolve a molecular boundary layer which perhaps would be a few millimetres thick. Instead, ν must be interpreted as some form of eddy viscosity, as we discuss in Chapter 13. In that case, one might argue that the free-slip condition should be preferred, but in the absence of a proper theoretical basis for such eddy viscosities there is no truly rational way to make the choice. We will solve the no-slip problem.

Let the wind stress be the canonical $\tau^x = -\cos(\pi y/a)$. Then the interior (Sverdrup) flow is given by (19.34), as for the Stommel problem. This satisfies the no-slip boundary conditions at $y = 0, 1$, namely $\partial_y \psi = 0$, automatically. However, we need boundary layers at both the western and eastern boundaries, because the interior solution cannot satisfy all four boundary conditions required by (19.42). The eastern boundary layer will be relatively weak, and needed only to satisfy the no-slip condition but, as in the Stommel problem, there will be a strong western boundary layer, needed to satisfy the no-normal flow condition. How thick will this be? Inspection of (19.42) suggests that the frictional term and the β term will balance in a boundary layer of thickness of order L_M where

$$L_M = \left(\frac{\nu}{\beta}\right)^{1/3}. \tag{19.43}$$

nondimensionalizing (19.42) in a similar way to the Stommel problem yields

$$-\epsilon_M \nabla^4 \widehat{\psi} + \frac{\partial \widehat{\psi}}{\partial \widehat{x}} = \mathrm{curl}_z \widehat{\boldsymbol{\tau}}_T, \tag{19.44}$$

where $\epsilon_M = (\nu/\beta a^3)$. Considering only the western boundary layer correction, we let the solution be the sum of an interior (Sverdrup) streamfunction plus a boundary layer correction:

$$\widehat{\psi} = \psi_I + \phi_W(\alpha, \widehat{y}), \tag{19.45}$$

where α is a stretched coordinate such that $\widehat{x} = \epsilon\alpha$ where ϵ is some small parameter. Substituting (19.45) into (19.44) and subtracting the Sverdrup balance gives

$$-\epsilon_M \left(\nabla^4 \psi_I + \frac{1}{\epsilon^4}\frac{\partial^4 \phi_W}{\partial \alpha^4}\right) + \frac{1}{\epsilon}\frac{\partial \phi_W}{\partial \alpha} = 0. \tag{19.46}$$

A non-trivial balance is obtained when $\epsilon = \epsilon_M^{1/3}$, implying a dimensional western boundary thickness of $\epsilon a = (\nu/\beta)^{1/3}$, consistent with (19.43). Equation (19.46) then becomes, at leading order,

$$-\frac{\partial^4 \phi_W}{\partial \alpha^4} + \frac{\partial \phi_W}{\partial \alpha} = 0. \tag{19.47}$$

The boundary conditions on (19.47) are that:

(i) $\phi_W \to 0$ as $\alpha \to \infty$: this states that the perturbation decays as it extends into the interior;

(ii) $\phi_W = -\psi_I$ at $\widehat{x} = \alpha = 0$: this is the no-normal-flow condition on the meridional boundary.

(iii) $\partial \phi_W/\partial \widehat{x} = -\partial \psi_I/\partial \widehat{x}$ at $\widehat{x} = \alpha = 0$: this is the no-slip condition.

In addition, zonal boundary layers must exist at $\widehat{y} = 0, 1$ and another meridional boundary layer must exist at $\widehat{x} = 1$, in order to satisfy the no slip condition. Solving the full problem is a straightforward albeit non-trivial algebraic exercise and, omitting the weak zonal boundary layers at $\widehat{y} = 0, 1$ but including the eastern boundary layer correction, we eventually find the solution

$$\widehat{\psi} = \psi_I - \mathrm{e}^{-\widehat{x}/(2\epsilon)}\left\{\psi_I(0,\widehat{y})\left[\cos\left(\frac{\sqrt{3}\widehat{x}}{2\epsilon}\right) + \frac{1}{\sqrt{3}}\sin\left(\frac{\sqrt{3}\widehat{x}}{2\epsilon}\right)\right] + \frac{2\epsilon}{\sqrt{3}}\sin\left(\frac{\sqrt{3}x}{2\epsilon}\right)\frac{\partial \psi_I}{\partial \widehat{x}}\bigg|_{x=0}\right\}$$
$$-\epsilon \mathrm{e}^{(\widehat{x}-1)/\epsilon}\frac{\partial \psi_I}{\partial \widehat{x}}\bigg|_{x=1}, \tag{19.48}$$

where $\epsilon = (\nu/\beta a^3)^{1/3}$. With the canonical wind stress, (19.27), the interior solution is given by

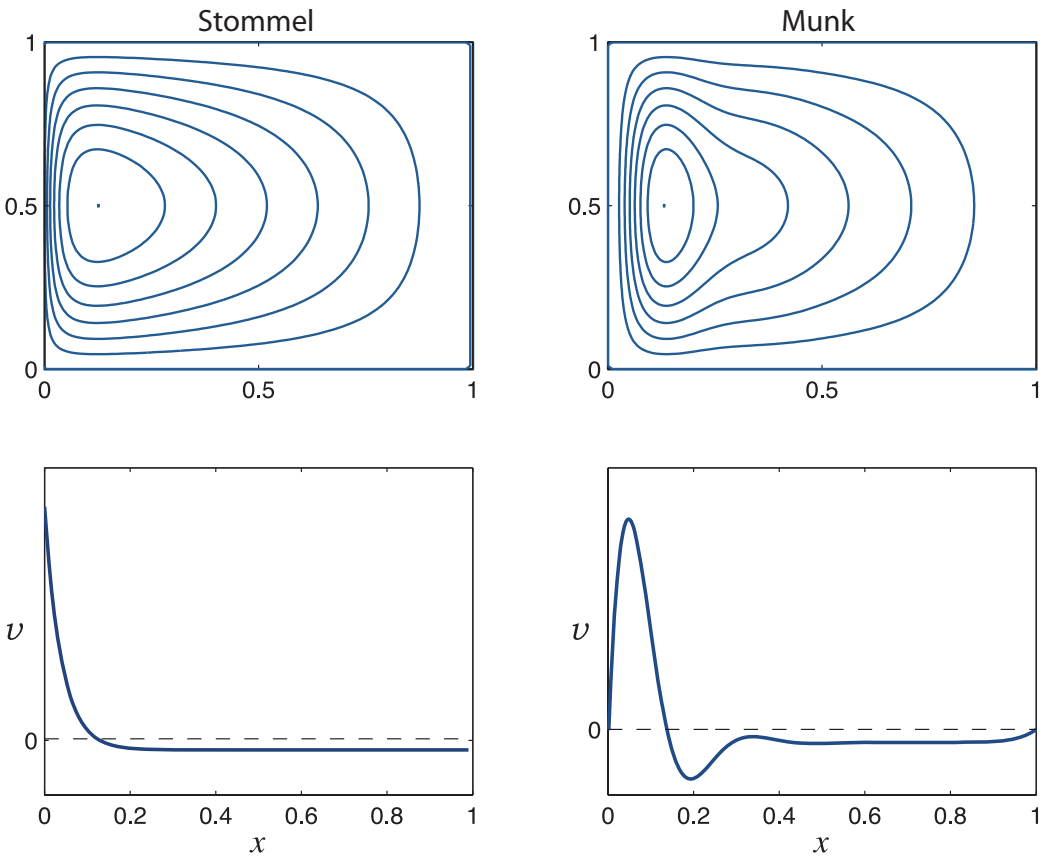

Fig. 19.7 The Stommel and Munk solutions, (19.49) with $\epsilon_S = \epsilon_M^{1/3} = 0.04$, with the wind stress $\tau = -\cos \pi y$, for $x, y \in (0, 1)$. Upper panels are contours of streamfunction in the x-y plane, and the flow is clockwise. The lower panels are plots of meridional velocity, v, as a function of x, in the centre of the domain ($y = 0.5$). The Munk solution can satisfy both no-normal flow and one other boundary condition at each wall, here chosen to be no-slip.

$\psi_I = \pi(1 - x) \sin \pi y$ and the above solution becomes

$$\widehat{\psi} = \pi \sin(\pi \widehat{y}) \left\{ 1 - \widehat{x} - \mathrm{e}^{-\widehat{x}/(2\epsilon)} \left[\cos\left(\frac{\sqrt{3}\widehat{x}}{2\epsilon} \right) + \frac{1 - 2\epsilon}{\sqrt{3}} \sin\left(\frac{\sqrt{3}\widehat{x}}{2\epsilon} \right) \right] + \epsilon \mathrm{e}^{(\widehat{x}-1)/\epsilon} \right\}. \qquad (19.49)$$

The solutions of this are plotted in Fig. 19.7. Note how the Munk layers bring the tangential as well as the normal velocity to zero. The eastern boundary layer has a similar thickness to the western boundary layer, but is not as dynamically important since its *raison d'etre* is to enable the no-slip condition to be satisfied, a relatively weak frictional constraint that manifests itself by a boundary layer in which the flow parallel to the boundary is slowed down. On the other hand the western boundary layer exists in order that the no-normal flow condition can be satisfied, which causes a qualitative change in the flow pattern. It should be emphasized that neither the Stommel nor the Munk models are accurate descriptors of the real ocean, but taken together the similarities of their solutions are a powerful argument for the relative insensitivity of the qualitative form of the solution to the detailed form of the friction. The models do in fact produce reasonably realistic patterns of large-scale flow in the major basins of the world, as illustrated in Fig. 19.8.

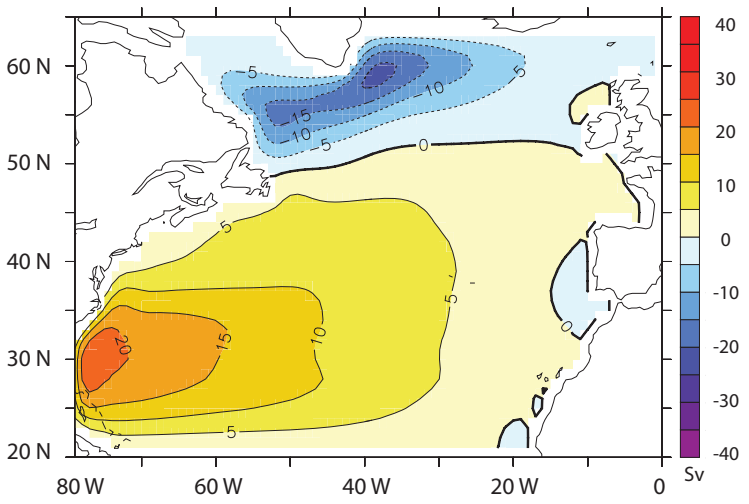

Fig. 19.8 The solution (streamfunction, in Sverdrups) to the Stommel–Munk problem numerically calculated for the North Atlantic, using the observed wind field. The model has realistic geometry, but is flat-bottomed.

The calculation reproduces the observed large-scale patterns, but the Gulf Stream and its extension are too diffuse, and its separation from the coast is a little too far north. Compare with Figs. 19.3 and 19.4.

19.3 ZONAL BOUNDARY LAYERS

The canonical wind stress $[\tau^x = -\tau_0 \cos(\pi y/a)]$ is special because its curl vanishes at $y = 0$ and a, and so the interior solution satisfies $\psi_I = 0$ at $y = 0$ and a. We cannot expect the real wind to be so accommodating. Consider, then, the Stommel problem forced by the linear wind profile,

$$\tau^x = \frac{\tau_0}{a}\left(y - \frac{a}{2}\right). \tag{19.50}$$

Scaling the variables in the usual way leads to the nondimensional problem

$$\epsilon_S \nabla^2 \widehat{\psi} + \frac{\partial \widehat{\psi}}{\partial \widehat{x}} = -1. \tag{19.51}$$

The interior flow obeys $\partial\widehat{\psi}/\partial\widehat{x} = -1$ everywhere, and evidently does not satisfy $\widehat{\psi} = 0$ at either $\widehat{y} = 0$ or $\widehat{y} = 1$; thus, boundary layers are needed at the meridional and zonal boundaries and we let the solution be the sum of five parts,

$$\widehat{\psi} = \psi_I + \phi_W + \phi_E + \phi_N + \phi_S, \tag{19.52}$$

with self-explanatory notation. The interior solution, ψ_I, is the solution of $\partial\psi_I/\partial\widehat{x} = -1$, so that a solution satisfying $\psi_I = 0$ at $\widehat{x} = 1$ is $\psi_I = (1 - \widehat{x})$ and there is no need for an eastern boundary layer. By the same methods we used in Section 19.1.3 the western boundary layer correction is easily found to be

$$\phi_W = -\mathrm{e}^{-\widehat{x}/\epsilon_S}. \tag{19.53}$$

It remains to find ϕ_N and ϕ_S, the boundary layer corrections at the northern and southern boundaries.

Consider the boundary layer correction at $y = 1$, and introduce the stretched coordinate α where $\epsilon'\alpha = y - 1$ and where ϵ' is a small parameter. Thus, we let $\phi_N = \phi_N(x, \alpha)$, and on substituting (19.52) into (19.51) we find

$$\epsilon_S\left(\nabla^2\psi_I + \frac{\partial^2\phi_N}{\partial\widehat{x}^2} + \frac{1}{\epsilon'^2}\frac{\partial^2\phi_N}{\partial\alpha^2}\right) + \frac{\partial\psi_I}{\partial\widehat{x}} + \frac{\partial\phi_N}{\partial\widehat{x}} = -1, \tag{19.54}$$

having neglected the small contributions from the other boundary layer streamfunctions (such as ϕ_S). To obtain a non-trivial balance we choose $\epsilon'^2 = \epsilon_S$ and obtain the dominant balance

$$\frac{\partial^2\phi_N}{\partial\alpha^2} + \frac{\partial\phi_N}{\partial\widehat{x}} = 0. \tag{19.55}$$

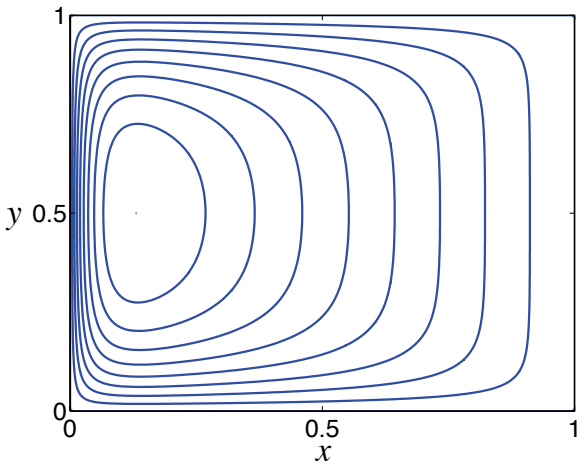

Fig. 19.9 Solutions to the Stommel problem with a wind stress that increases linearly from $y = 0$ to $y = 1$, as in (19.50). The interior solution is $\psi_I = (1 - x)$, or $v_I = -1$, necessitating zonal boundary layers at $y = 0$ and $y = 1$, as well as a western boundary layer at $x = 0$.

The boundary conditions necessary to complete the solution are:

(i) The total streamfunction (interior plus boundary correction) must vanish at the northern boundary; that is, $\phi_N(\hat{x}, \alpha = 0) = -\psi_I(\hat{x}, \hat{y} = 1) = -(1 - \hat{x})$.

(ii) The boundary solution should match to the interior streamfunction far from the boundary; that is $\phi_N(\hat{x}, \alpha \to -\infty) = 0$.

(iii) At the eastern boundary ϕ_N should also vanish, for otherwise it would provide a velocity into the eastern wall; that is $\phi_N(1, \alpha) = 0$.

The solution at the southern boundary is obtained in an analogous way, and the complete solution is illustrated in Fig. 19.9 (obtaining the solution analytically is quite algebraically tedious and is easier done numerically). The nondimensional thickness of the zonal (northern and southern) boundary layers is $\epsilon_S^{1/2}$, which, because it scales like the half power of a small number, is much thicker than the western boundary current. The thickness arises from the dimensional equations that dominate at the boundary, namely

$$r\frac{\partial^2 \psi}{\partial y^2} + \beta\frac{\partial \psi}{\partial x} = 0. \tag{19.56}$$

This follows from (19.18) by noting that the Laplacian operator must be dominated by the derivatives in the y-direction, and the β term has an (interior) component that annihilates the wind-stress curl, plus a boundary layer correction to balance the Laplacian. Inspection of (19.56) yields a dimensional thickness $L_Z \sim \sqrt{ra/\beta} = \epsilon_S^{1/2} a$, where a is the length scale in the x-direction.

19.4 ✦ THE NONLINEAR PROBLEM

In the nonlinear problem we seek solutions to

$$\frac{\partial \zeta}{\partial t} + J(\psi, \zeta) + \beta\frac{\partial \psi}{\partial x} = -r\nabla^2\psi + \mathrm{curl}_z \boldsymbol{\tau}_T + \nu\nabla^2\zeta, \tag{19.57}$$

which we have written in dimensional form. In the Stommel problem we set $\nu = 0$ and in the Munk problem we set $r = 0$. In general, solutions will be time-dependent and turbulent and this will create motion on small scales, so that ν cannot be neglected. The 'steady nonlinear Stommel–Munk problem' is

$$J(\psi, \zeta) + \beta\frac{\partial \psi}{\partial x} = -r\nabla^2\psi + \mathrm{curl}_z \boldsymbol{\tau}_T + \nu\nabla^2\zeta. \tag{19.58}$$

We can scale this by first supposing that the leading order balance is Sverdrupian (i.e., $\beta\partial\psi/\partial x \sim \mathrm{curl}_z \boldsymbol{\tau}_T$), from which we obtain the scales $\Psi = |\tau|/\beta$ and $U = |\tau|/(\beta L)$. Equation (19.58) may then be nondimensionalized to yield

$$R_\beta J(\widehat{\psi},\widehat{\zeta}) + \frac{\partial\widehat{\psi}}{\partial\widehat{x}} = -\epsilon_S\nabla^2\widehat{\psi} + \mathrm{curl}_z\widehat{\boldsymbol{\tau}}_T + \epsilon_M\nabla^2\widehat{\zeta}, \tag{19.59}$$

where $R_\beta = U/\beta L^2 = |\tau|/(\beta^2 L^3)$, the β-Rossby number for this problem, is a measure of the nonlinearity. Evidently, the nonlinear term increases in importance with increasing wind stress and for a smaller domain.

19.4.1 A Perturbative Approach

A direct attack on the full nonlinear problem (19.58) is possible only through numerical methods, so first we shall explore the problem perturbatively, assuming the nonlinear term to be small; the analysis is straightforward, albeit messy. We begin with the Stommel problem, (19.59) with $\epsilon_M = 0$, and expand the streamfunction in terms of R_β,

$$\widehat{\psi} = \psi_0 + R_\beta\psi_1 + \ldots . \tag{19.60}$$

Now substitute this into (19.59) and equate powers of R_β. The lowest-order problem is simply

$$\epsilon_S\nabla^2\psi_0 + \frac{\partial\psi_0}{\partial\widehat{x}} = \mathrm{curl}_z\widehat{\boldsymbol{\tau}} \tag{19.61}$$

which is the Stommel problem we have already solved. At the next order,

$$\epsilon_S\nabla^2\psi_1 + \frac{\partial\psi_1}{\partial\widehat{x}} = J(\psi_0,\zeta_0). \tag{19.62}$$

This equation has precisely the same form as the Stommel problem, with the known nonlinear term on the right-hand side playing the part of the wind stress. The algebra to obtain the solution is rather tedious, because the right-hand side varies with both $\widehat{x}$ and $\widehat{y}$, but this is much ameliorated by the use of computer algebraic manipulation languages. For the canonical wind stress $\tau^x = -\tau_0\cos(\pi\widehat{y})$ the corrected solution, in the boundary layer approximation and ignoring any corrections at the zonal boundaries, is found to be[10]

$$\widehat{\psi} \approx \sin(\pi\widehat{y})(1-\widehat{x}-\mathrm{e}^{-\widehat{x}/\epsilon_S}) - \frac{R_\beta\pi^3}{2\epsilon_S^3}\sin(2\pi\widehat{y})\widehat{x}\mathrm{e}^{-\widehat{x}/\epsilon_S}. \tag{19.63}$$

The solution is illustrated in Fig. 19.10. The perturbation is antisymmetric about $\widehat{y} = 1/2$, being positive for $\widehat{y} > 1/2$ and negative for $\widehat{y} < 1/2$. This tends to move the centre of the gyre polewards, narrowing and intensifying the flow in the poleward half of the western boundary current, whereas the western boundary current equatorwards of $\widehat{y} = 1/2$ is broadened and weakened. The net effect is that the centre of the gyre is pushed poleward — essentially because the western boundary current is advecting the vorticity of the gyre poleward. In the perturbation solution the advection is both by and of the linear Stommel solution; thus, negative vorticity is advected polewards, intensifying the gyre in its poleward half, weakening it in its equatorward half. The solution illustrated in Fig. 19.10 has $\epsilon = 0.04$ and $R_\beta = 10^{-4}$; for larger values of R_β the perturbation itself starts to dominate.

The problem with this perturbative approach is that a boundary layer solution to the Stommel problem does not calculate derivatives accurately, so that the nonlinear term $J(\psi,\nabla^2\psi)$ is poorly approximated in the western boundary layer; however, in the interior where the errors are small the perturbative correction is negligible. A more accurate perturbative approach begins with the *exact* solution to the Stommel problem, and then proceeds in the same way. However, the analytic effort is considerable, and the intuitive sense of the way nonlinearities affect the solution is not apparent.

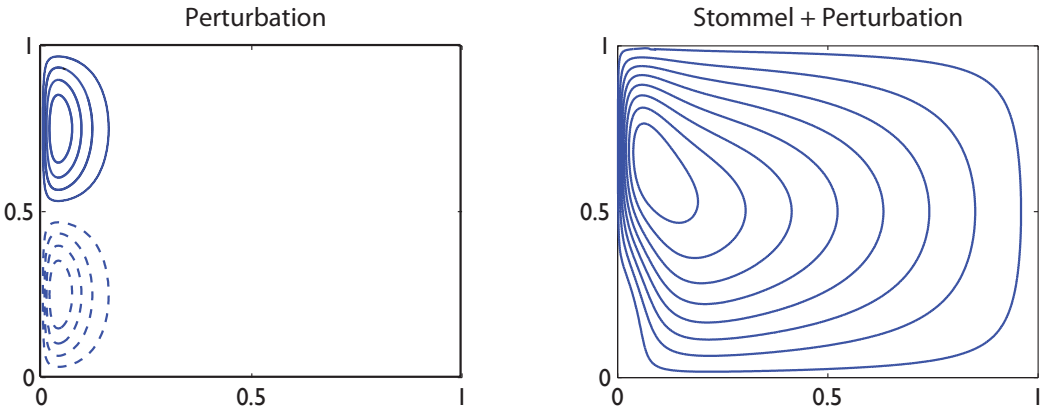

Fig. 19.10 The nonlinear perturbation solution of the Stommel problem, calculated according to (19.63). On the left is the perturbation, $-R_\beta \pi^3/(2\epsilon_S^2)\sin(2\pi y) x e^{-x/\epsilon_S}$, and on the right is the reconstituted solution, using $R_\beta = 10^{-4}$ and $\epsilon = 0.04$. Dashed contours are negative.

19.4.2 A Numerical Approach

Fully nonlinear solutions show qualitatively similar effects to those seen in the perturbative solutions, as we see in Fig. 19.11, where the solutions to (19.59) for the Stommel and Munk problems are obtained numerically by Newton's method.[11]

Just as with the perturbative procedure, for both the Stommel and Munk problems small values of nonlinearity lead to the poleward advection of the gyre's anticyclonic vorticity in the western boundary current, strengthening and intensifying the boundary current in the northwest corner. A higher level of nonlinearity results in a strong recirculating regime in the upper westward quadrant, and ultimately much of the gyre's transport is confined to this regime. The western boundary current itself becomes less noticeable as nonlinearity increases, the more nonlinear solutions have a much greater degree of east-west symmetry than the linear ones, just as the fully nonlinear Fofonoff solutions (Section 19.5.3).

The qualitative effects above do not depend on the precise formulation of the model, but the boundary conditions do play an important role in the detailed solution. For example, for a given value of R_β, nonlinearity has a stronger effect in the Munk problem with slip boundary conditions than with no-slip, because in the latter the velocity is reduced to zero at the boundary with a corresponding reduction in the advection term. However, these solutions themselves are unlikely to be relevant for larger values of nonlinearity, because then the flow becomes hydrodynamically unstable

19.5 ✦ INERTIAL SOLUTIONS

In this section we further explore inertial effects and ask: might purely inertial effects be sufficient to satisfy boundary conditions at the western boundary? Can we envision a purely inertial gyre circulation? Our question is motivated by the steady wind-driven, Rayleigh-damped quasi-geostrophic equation, namely

$$J(\psi, \nabla^2\psi) + \beta \frac{\partial \psi}{\partial x} = F_\tau - r\nabla^2\psi, \tag{19.64}$$

where F_τ is the wind forcing. Since the inertial (advective) terms are of a higher order than the linear terms, indeed they are of a higher order than the Rayleigh drag, it is natural to wonder if they themselves might serve to satisfy the no-normal flow condition on the western boundary, without

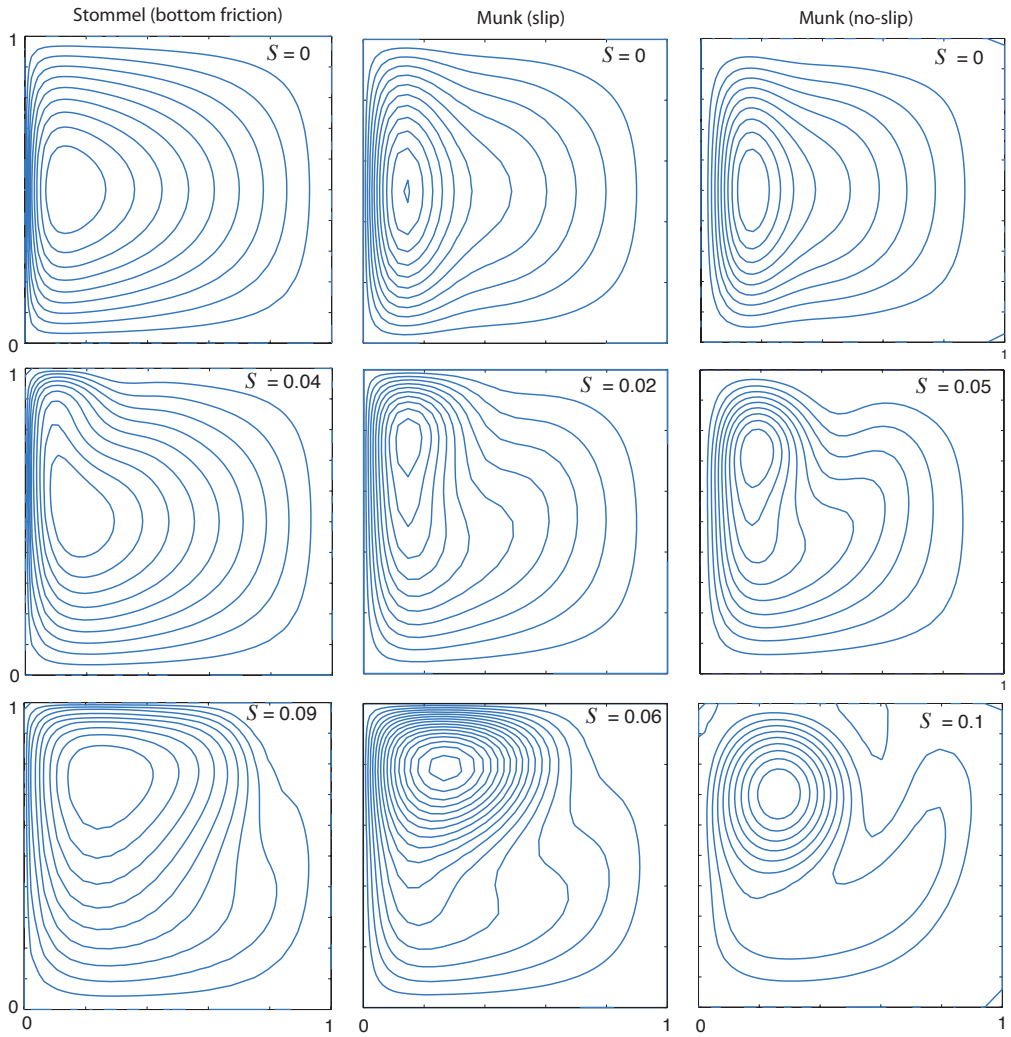

Fig. 19.11 Streamfunctions in solutions of the nonlinear Stommel and Munk problems, obtained numerically with a Newton's method, for various values of the nonlinearity parameter $S = R_\beta^{1/2}$. As in the perturbation solution, for small values of nonlinearity the centre of the gyre moves polewards, strengthening the boundary current in the north-western quadrant (for a northern-hemisphere solution). As nonlinearity increases, the recirculation of the gyre dominates, and the solutions become increasingly inertial.[12]

recourse to rather ill-defined frictional terms. The answer is no, as we see below, but nevertheless nonlinear effects may be important in the western boundary layer even if they are small in the interior.

19.5.1 The Need for Friction

Consider the steady barotropic flow satisfying

$$\boldsymbol{u} \cdot \nabla q = \mathrm{curl}_z \boldsymbol{\tau}_T + \mathrm{Fr}, \tag{19.65}$$

where $q = \nabla^2\psi + \beta y$ and Fr represents frictional effects. Noting that $\boldsymbol{u}$ is divergence-free and integrating the left-hand side of (19.65) over the area, A, between two closed streamlines (ψ_1 and

ψ_2, say) and using the divergence theorem we find

$$\int_A \nabla \cdot (\boldsymbol{u}q)\ \mathrm{d}A = \oint_{\psi_1} \boldsymbol{u}q \cdot \boldsymbol{n}\,\mathrm{d}l - \oint_{\psi_2} \boldsymbol{u}q \cdot \boldsymbol{n}\,\mathrm{d}l = 0. \tag{19.66}$$

Here, $\boldsymbol{n}$ is the unit vector normal to the streamline so that $\boldsymbol{u} \cdot \boldsymbol{n} = 0$. The integral of the wind-stress curl over the same area will not, in general, be zero. Now, we can take these two streamlines as close together as we wish; thus, a balance in (19.65) can only be achieved if *every* closed contour passes through a region where frictional effects are non-zero. This does not mean that nonlinear terms may not locally dominate the friction, just that friction must be somewhere important. In the Stommel and Munk problems, it means that every streamline must pass through the frictional western boundary layer.

Frictional and inertial scales

The ratio of the size of the nonlinear terms to the linear terms is given by the β-Rossby number, $R_\beta = U/(\beta L^2)$. In the western boundary layer the length scales can be expected to be much smaller than the basin scale, and if the balance in the western boundary layer were between the nonlinear and beta term, as in

$$u\frac{\partial}{\partial x}\nabla^2\psi \sim \beta\frac{\partial \psi}{\partial x}, \tag{19.67}$$

then the *inertial boundary layer thickness*, δ_I, is given by

$$\delta_I = \left(\frac{U}{\beta}\right)^{1/2}. \tag{19.68}$$

This, of course, gives $R_\beta = 1$ if $L = \delta_I$. The more energetic the flow, the wider the region where nonlinearity is important, and the corresponding scale is sometimes called the Charney thickness.[13]

The linearized Stommel equation has a boundary layer of dimensional thickness of order $\delta_S = (r/\beta)$, obtained by equating $\beta\,\partial\psi/\partial x$ and $r\nabla^2\psi$. This thickness is equal to the inertial boundary layer thickness when $U = (r^2/\beta)$. If $\delta_I > \delta_S$, i.e., if $U > (r^2/\beta)$, then nonlinearity *must* be important in the western boundary layer, because the nonlinear terms are at least as important as the beta term in (19.64). On the other hand, if the Stommel boundary layer is wider than the inertial boundary layer, there is no obvious need for nonlinearity to be important, since the Stommel boundary layer generates no length scales smaller than δ_I and R_β remains small.

19.5.2 Attempting an Inertial Western Boundary Solution

Although friction must be important, it is nevertheless instructive to try to find a purely inertial solution for the western boundary layer, and to see if and how the attempt fails. Let us suppose that the interior solution has purely zonal flow, with flow either towards or away from the western boundary current, and consider the dimensional equation of motion

$$J(\psi, \nabla^2\psi + \beta y) = 0. \tag{19.69}$$

This has the general solution

$$\nabla^2\psi + \beta y = G(\psi), \tag{19.70}$$

where G is an arbitrary function of its argument. Consider first the case with flow entering the boundary layer with a local velocity $-U$ (i.e., westward); that is, $\psi = Uy$. The potential vorticity in this region (just outside our putative boundary layer) is $Q_I = \beta y$. Thus, the relation between potential vorticity and streamfunction is $Q_I = \beta\psi_I/U$ and so

$$G(\psi) = \frac{\beta\psi}{U}. \tag{19.71}$$

Because we are assuming the flow is inviscid, the fluid will preserve this relationship between potential vorticity and streamfunction *even as it moves through the western boundary layer.* Thus, using (19.70) and (19.71), the flow in the interior *and* in the boundary layer is given by the solution of

$$\nabla^2\psi - \frac{\beta\psi}{U} = -\beta y, \tag{19.72}$$

with $\psi = 0$ on the boundary. To obtain a solution, we let $\psi = \psi_I + \phi$, where $\psi_I = U y$ is the particular solution to (19.72) (and, of course, the interior flow). The boundary layer correction then obeys

$$\nabla^2\phi - \frac{\beta\phi}{U} = 0, \tag{19.73}$$

with $\phi = -\psi_I$ at $x = 0$. Now, in the boundary layer, length scales in the x-direction are much smaller than length scales in the y-direction, and so (19.73) becomes approximately

$$\frac{\partial^2\phi}{\partial x^2} - \frac{\beta\phi}{U} = 0. \tag{19.74}$$

(We could formalize this procedure by nondimensionalizing and introducing a stretched coordinate, as we did for the Stommel problem.) Solutions of (19.74) are $\phi = -\psi_I e^{-x/\delta_I}$, where $\delta_I = (U/\beta)^{1/2}$, and so the full solution is

$$\psi = \psi_I(1 - e^{-x/\delta_I}). \tag{19.75}$$

Clearly, this solution smoothly transitions into the interior solution for large x.

What about solutions exiting the boundary layer? We might attempt a similar procedure, but now the interior boundary condition that we must match is that of eastward flow, namely $\psi_I = -U y$. Thus, analogously to (19.72), we seek solutions to the problem,

$$\nabla^2\psi + \frac{\beta\psi}{U} = -\beta y, \tag{19.76}$$

for which the homogeneous (boundary layer) equation is

$$\frac{\partial^2\phi}{\partial x^2} + \frac{\beta\phi}{U} = 0. \tag{19.77}$$

Solutions of (19.77) are

$$\psi = \psi_I(1 - e^{-x/\delta_I^*}), \tag{19.78}$$

where $\delta_I^* = i\,\delta_I = i\,(U/\beta)^{1/2}$, and may be compared with (19.75). The solution is therefore wave-like, and does not transition smoothly to the interior flow. This suggests that friction must be important in allowing the boundary layer to smoothly connect to the interior for reasons connected to the conservation of potential vorticity, as explained heuristically in the next subsection.[14]

In addition to this transition problem, we note that (19.75) and (19.78) together do not constitute a globally acceptable inviscid solution, for the simple reason that the flow in the westward flowing interior region has a different potential vorticity–streamfunction (q–ψ) relationship than does the eastwards flowing interior. If these two regions are connected by a boundary layer, the flow in that boundary layer must be viscous or unsteady since the value of potential vorticity on the streamlines has changed, whereas inviscid flow conserves potential vorticity.

The connection between the boundary layer and the interior

We have seen that solutions with a boundary layer character that blend smoothly to a flow interior exist only for westward interior flow ($u_I = -U < 0$): an inertial western boundary layer on a beta-plane evidently cannot easily release fluid into the interior. The underlying reason for this stems from the conservation of potential vorticity, as we now explain (and see Fig. 19.12).

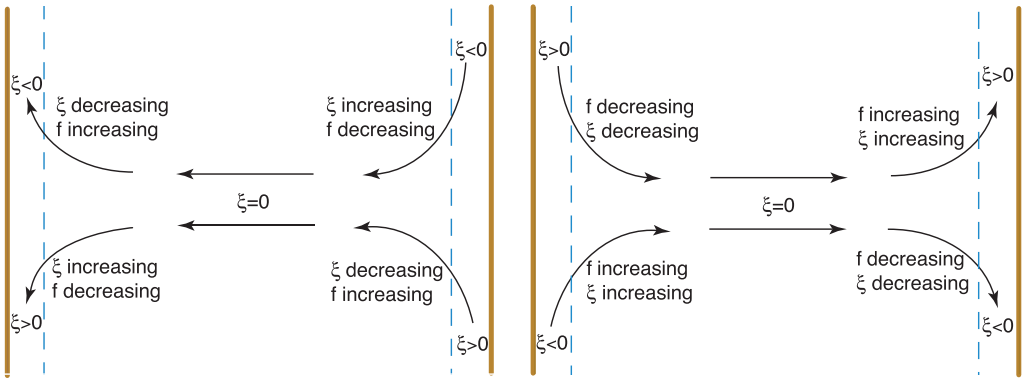

Fig. 19.12 Putative inertial boundary layers connected to a westward flowing interior flow (left panel) or eastwards flowing interior flow (right panel), in the Northern Hemisphere. Westward flow into the western boundary layer, or flow emerging from an eastern boundary layer, is able to conserve its potential vorticity through a balance between changes in relative vorticity and Coriolis parameter. But flow cannot emerge smoothly from a western boundary layer into an eastwards flowing interior and still conserve its potential vorticity. The right panel thus has inconsistent dynamics.

Conservation of potential vorticity demands that, in barotropic flow, $v_x - u_y + \beta y$ is a constant on streamlines. In the interior, relative vorticity, ζ, is zero, and in the meridional boundary layers it is effectively v_x. Consider first the case with westward flow in the interior (left panel of Fig. 19.12). Fluid from the irrotational interior approaches the western boundary where it is deflected either polewards or equatorwards. In the former case its relative vorticity falls, so allowing potential vorticity to be conserved because the reduction of ζ can be balanced by an increase in the planetary vorticity, f. Similarly, flow deflected southwards produces positive relative vorticity, which is compensated for by the reduced value of f. In the eastern boundary layer, southwards (northwards) moving flow has negative (positive) relative vorticity. As it emerges into the interior its relative vorticity increases (decreases), this being balanced by a fall (rise) in the value of f. Thus, we see that the solution with a westward flowing interior can indeed conserve potential vorticity, at both eastern and western boundaries.

On the other hand suppose the interior flow were eastwards (right panel of Fig. 19.12). Flow moving polewards in the western boundary layer has negative relative vorticity. It cannot be freely released into an irrotational interior because f and ζ would then both need to increase, violating potential vorticity conservation. Flow moving southwards with positive relative vorticity similarly is trapped within the western boundary current, unless it meets a zonal boundary which allows an eastward moving boundary current with positive relative vorticity. Similar arguments show that an eastern boundary current cannot entrain fluid from an eastward flowing irrotational interior.

One might ask, why cannot we simply reverse the trajectory of all the fluid parcels in an inviscid flow and thereby obtain a solution with an eastward-flowing interior? The answer is that such a flow will only be a solution if we also reverse the direction of the Earth's rotation, and so reverse the sign of β, and hence the location of the frictional boundary current.

19.5.3 A Fully Inertial Approach: the Fofonoff Model

Rather than attempt to match an inertial boundary layer with an interior Sverdrup flow, we may look for a purely inertial solution that holds basinwide, and such a construction is known as the *Fofonoff model*.[15] That is, we seek global solutions to the inviscid, unforced problem,

$$J(\psi, \nabla^2\psi + \beta y) = 0. \tag{19.79}$$

We should not regard this problem as representing even a very idealized wind-driven ocean; rather, we may hope to learn about the properties of purely inertial solutions and this might, in turn, tell us something about the ocean circulation.

The general solution to (19.79) is

$$\nabla^2\psi + \beta y = Q(\psi), \tag{19.80}$$

where $Q(\psi)$ is an arbitrary function of its argument. For simplicity we choose the linear form,

$$Q(\psi) = A\psi + B, \tag{19.81}$$

where $A = \beta/U$ and $B = \beta y_0$, where U and y_0 are arbitrary constants. Thus, (19.80) becomes

$$\left(\nabla^2 - \frac{\beta}{U}\right)\psi = \beta(y_0 - y). \tag{19.82}$$

We will further choose $\beta/U > 0$, which we anticipate will provide a westward-flowing interior flow, and which (from our experience in the previous section) is more likely to provide a meaningful solution than an eastward interior, and we will use boundary-layer methods to find a solution. A natural scaling for ψ is UL, where L is the domain size, and with this the nondimensional problem is

$$(\epsilon_F\nabla^2 - 1)\widehat{\psi} = \widehat{y}_0 - \widehat{y}, \tag{19.83}$$

where $\epsilon_F = U/(\beta L^2)$ and $\widehat{y} = y/L$. If we take ϵ_F to be small (note that $\epsilon_F = R_\beta$) we can find a solution by boundary-layer methods similar to those used in Section 19.1.3 for the Stommel problem. Thus, we write $\widehat{\psi} = \widehat{\psi}_I + \widehat{\phi}$ where $\widehat{\psi}_I = \widehat{y} - \widehat{y}_0$ (dimensionally, $\psi_I = U(y - y_0)$) and $\widehat{\phi}$ is the boundary layer correction, to be calculated separately for each boundary using

$$\epsilon_F\nabla^2\widehat{\phi} - \widehat{\phi} = 0 \tag{19.84}$$

and the boundary condition that $\widehat{\phi} + \widehat{\psi}_I = 0$. For example, at the northern boundary, $\widehat{y} = \widehat{y}_N$, the y-derivatives will dominate and (19.84) may be approximated by

$$\epsilon_F\frac{\partial^2\widehat{\phi}}{\partial\widehat{y}^2} - \widehat{\phi} = 0, \tag{19.85}$$

with solution

$$\widehat{\phi} = B\exp[-(\widehat{y}_N - \widehat{y})/\epsilon_F^{1/2}], \tag{19.86}$$

where $B = \widehat{y}_0 - \widehat{y}_N$, hence satisfying the boundary condition that $\widehat{\phi}(\widehat{x}, \widehat{y}_N) = -\widehat{\psi}_I(\widehat{x}, \widehat{y}_N)$. We follow a similar procedure at the other boundaries to obtain the full solution, and in dimensional form this is

$$\psi = U(y - y_0)\left[1 - \mathrm{e}^{-x/\delta_I} - \mathrm{e}^{-(x_E - x)/\delta_I}\right] + U(y_0 - y_N)\mathrm{e}^{-(y_N - y)/\delta_I} + Uy_0\mathrm{e}^{-y/\delta_I}, \tag{19.87}$$

where $\delta_I = (U/\beta)^{1/2}$ is the boundary layer thickness. Evidently, only positive values of U corresponding to a westward interior flow give boundary-layer solutions that decay into the interior.

A typical solution is illustrated in Fig. 19.13. On approaching the western boundary layer, the interior flow bifurcates at $y = y_0$. The western boundary layer, of width δ_I, accelerates away from this point, being constantly fed by the interior flow. The westward return flow occurs in zonal boundary layers at the northern and southern edges, also of width δ_I. Flow along the eastern boundary layers is constantly being decelerated, because it is feeding the interior. If one of the zonal boundaries corresponds to y_0 (e.g., if $y_N = y_0$) there would be no boundary layer along it, since ψ is already zero at $y = y_0$. Rather, there would be westward flow along it, just as in the interior. Indeed, a slippery wall placed at $y = 0.5$ would have no effect on the solution illustrated in Fig. 19.13.

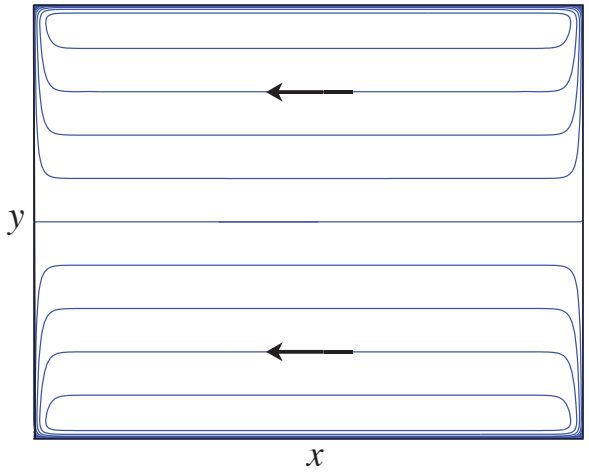

Fig. 19.13 The Fofonoff solution. Plotted are contours (streamlines) of (19.87) in the plane $0 < x < x_E$, $0 < y < y_N$ with $U = 1$, $y_N = 1$, $x_E = y_N = 1$, $y_0 = 0.5$ and $\delta_I = 0.05$. The interior flow is westward everywhere, and $\psi = 0$ at $y = y_0$. In addition, boundary layers of thickness $\delta_I = \sqrt{U/\beta}$ bring the solution to zero at $x = (0,\ x_E)$ and $y = (0,\ y_N)$, excepting small regions at the corners.

19.6 ✦ TOPOGRAPHIC EFFECTS ON WESTERN BOUNDARY CURRENTS

The above sections have emphasized the role of friction in satisfying the boundary conditions in the west. However, we should certainly not think of friction as being the *cause* of the western boundary layer and in this section we shall show that if there are sloping sidewalls the role of friction is significantly different, and the western boundary current may even be largely inviscid![16] The key point is that the flow may be inviscid if it is able to follow potential vorticity contours. In a flat-bottomed western boundary layer the flow is moving to larger values of f (and not as a direct response to the wind) and so the flow *must* be frictional. However, if the sidewalls are sloping, then the flow may preserve its potential vorticity (approximately, its value of f/h) if it moves offshore as it moves polewards. In the treatment below, we focus on homogeneous fluids, noting that the interaction of topography and stratification is a subtle and rather complex problem.

19.6.1 Homogeneous Model

The potential vorticity evolution equation for a homogeneous model with topography and a rigid lid may be written as:

$$\frac{\mathrm{D}q}{\mathrm{D}t} = \frac{F}{h}, \tag{19.88}$$

where $q = (\zeta + f)/h$ where $h = h(x, y)$ is the time-independent depth of the fluid, and F represents vorticity forcing and frictional terms. The advecting velocity is determined by noting that the mass conservation equation is just $\nabla \cdot [\boldsymbol{u}h(x, y)] = 0$, which allows us to define the mass-transport streamfunction ψ such that

$$u = -\frac{1}{h}\frac{\partial \psi}{\partial y}, \qquad v = \frac{1}{h}\frac{\partial \psi}{\partial x}. \tag{19.89}$$

The streamfunction itself is obtained from the vorticity by solving the elliptic equation,

$$\nabla \cdot \left(\frac{1}{h}\nabla \psi\right) = \zeta = qh - f. \tag{19.90}$$

Equations (19.88), (19.90) and (19.89) form a closed system. Unlike the quasi-geostrophic case, neither the Rossby number nor the topography need be small for the model to be valid. Including finite size topography but not stratification is not especially realistic *vis-à-vis* the real ocean, but nevertheless this model is physically realizable and a useful tool.

The 'topographic Stommel problem' is obtained by neglecting relative vorticity in the potential vorticity in (19.88) (i.e., let $q = f/h$) and using a linear drag acting on the vertically integrated fields

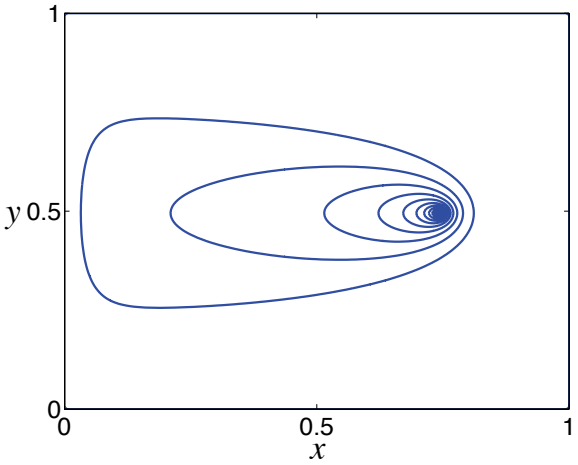

Fig. 19.14 The β-plume, namely the Green function for the Stommel problem. Specifically we plot the solution of (19.93) with $\psi = 0$ at the walls, and a delta-function source at $x = 0.75,\ y = 0.5$.

The streamfunction trails westward from the source, as if it were a tracer being diffused while being advected westward along lines of constant f.

for friction, and a wind-stress curl forcing. Multiplying (19.88) by h, expanding the advective term and omitting time dependence gives

$$J\left(\psi, \frac{f}{h}\right) = -r\nabla^2\psi + \mathrm{curl}_z(\boldsymbol{\tau}_T/h), \tag{19.91}$$

where the boundary conditions are $\psi = 0$ at the domain edges and $\boldsymbol{\tau}_T$ represents the wind stress at the top.

19.6.2 Advective Dynamics

An illuminating way to begin to study the problem is to write (19.91) in the form[17]

$$J(\Psi, \psi) = +r\nabla^2\psi - \mathrm{curl}_z(\boldsymbol{\tau}_T/h), \tag{19.92}$$

where $\Psi \equiv f/h$. Thus, noting that $J(\Psi, \psi) = \boldsymbol{U} \cdot \nabla\psi$ where $\boldsymbol{U} = \mathbf{k} \times \nabla(f/h)$, we regard ψ as being advected by the pseudovelocity $\boldsymbol{U}$. This advection is along f/h contours and is quasi-westward, meaning that high values of potential vorticity lie to the right. Equation (19.92) is then an advection-diffusion equation for the tracer ψ, with the 'source' of ψ being the wind stress curl with ψ being diffused by the first term on the right-hand side of (19.92), and advected by $\boldsymbol{U}$. This same interpretation applies to the original Stommel problem, of course, where the pseudovelocity, $-\beta\mathbf{i}$, is purely westward, and it is useful to first revisit this problem.

Consider, then, a flat-bottomed ocean, where the wind-stress curl is just a point source at $\boldsymbol{x}_0$. With $\Psi = f$, (19.92) becomes

$$r\nabla^2\psi + \beta\frac{\partial\psi}{\partial x} = \delta(\boldsymbol{x} - \boldsymbol{x}_0). \tag{19.93}$$

This can be transformed to a Helmholtz equation by writing $\phi = \psi \exp(\beta x/2r)$, giving $\nabla^2\phi - [\beta/(2r)]^2\phi = \delta(\boldsymbol{x} - \boldsymbol{x}_0)$. This may then be solved exactly, and the solution (for ψ) is illustrated in Fig. 19.14 — this is the Green function for the Stommel problem. The tracer ψ is 'advected' westward along f/h contours — lines of latitude in this case — spreading diffusively as it goes; the resulting structure is called a *β-plume*. The western boundary layer results as a consequence of the f/h contours colliding with the western boundary, along with the need to satisfy the boundary condition $\psi = 0$. If there were no diffusion at all, ψ would just propagate westward from the source, and if in addition the source were spatially distributed, for example as $\sin \pi y$, the solution streamfunction would represent Sverdrup interior flow. This case is illustrated in Fig. 19.15(a), which

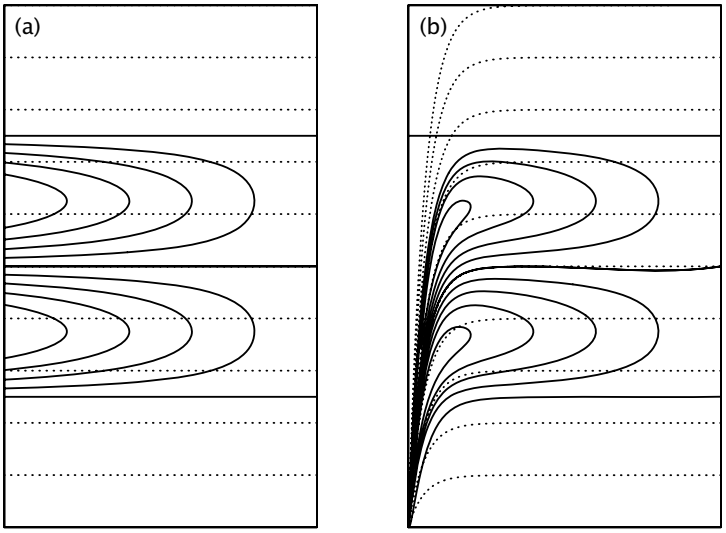

Fig. 19.15 The two-gyre Sverdrup flow (solid contours) for (a) a flat-bottomed domain, and (b) a domain with sloping sidewalls. The f/h contours are dotted.[18]

shows the solution to (19.93) with $r = 0$ and with the right-hand side replaced by a conventional 'two-gyre' wind stress.

Now consider the case with a sloping sidewall on the western boundary. The f/h contours (the dotted lines in Fig. 19.15b) tend to converge at the southwest corner of the domain, and only where f/h contours intersect the boundary is a diffusive boundary layer required. In terms of the interpretation above, wind stress provides a source for the streamfunction ψ and the latter is advected *pseudowestward* — i.e., along potential vorticity contours, with higher values to the right. The source in this case is distributed over the entire domain, but the contours all converge in the southwest corner. The (numerically obtained) solution to the associated Stommel problem is illustrated in Fig. 19.16, and the western boundary current in this case is no longer a frictional boundary layer. Friction is necessarily important where the flow crosses f/h contours; linear theory suggests that this will occur at the southwest corner. It also occurs on the western boundary where the f/h contours are densely packed and the vorticity in the topographic Sverdrup flow is large, and the friction enables the flow to move across the f/h contours. (In the flat bottomed case the f/h contours are zonal and friction allows the flow to move meridionally.)

19.6.3 Bottom Pressure Stress and Form Drag

In the homogeneous problem f and h appear only in the combination f/h, and we may solve the problem entirely without considering pressure effects. It is nevertheless informative to think about how the pressure interacts with the topography to produce meridional flow, and as a way toward addressing the effects of stratification. The geostrophic momentum equation is

$$\boldsymbol{f} \times \boldsymbol{u} = -\nabla\phi + \boldsymbol{F}, \tag{19.94}$$

where $\boldsymbol{F}$ represents both wind forcing and frictional terms. Integrating this over the depth of the ocean (with $z = 0$ at the top), and using the Leibnitz rule ($\nabla \int_{\eta_B}^{0} \phi \, dz = \int_{\eta_B}^{0} \nabla\phi \, dz - \phi_B \nabla\eta_B$) to evaluate the pressure term, gives

$$\boldsymbol{f} \times \overline{\boldsymbol{u}} = -\nabla\overline{\phi} - \phi_B \nabla\eta_B + \overline{\boldsymbol{F}}. \tag{19.95}$$

Here, the overbar denotes a vertical integral (e.g., $\overline{\boldsymbol{u}} = \int_{\eta_B}^{0} \boldsymbol{u} \, dz$), ϕ_B is the pressure at $z = \eta_B$ and η_B is the z-coordinate of the bottom topography. We take the top of the ocean at $z = 0$, and note

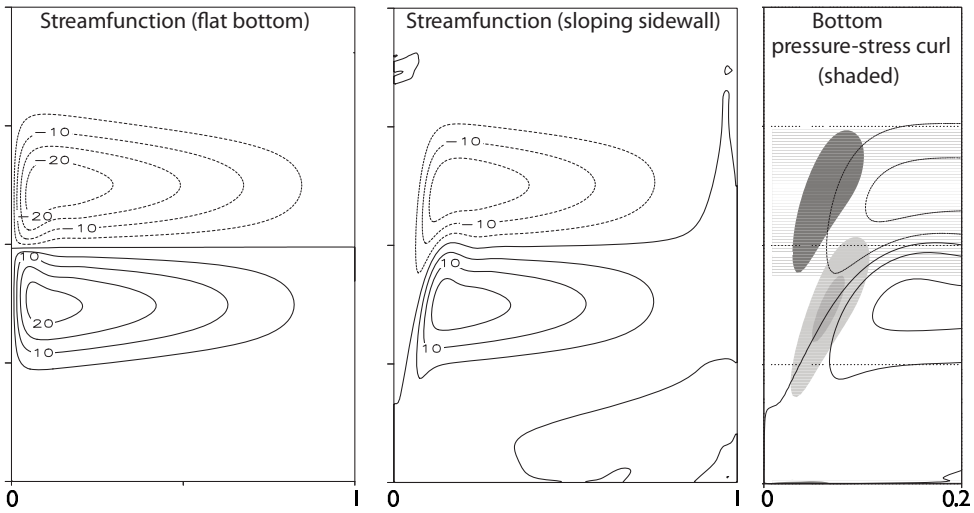

Fig. 19.16 The numerically obtained steady-state solution to the homogeneous problem with a two-gyre forcing and friction, for a flat-bottomed domain and a domain with sloping western sidewall. The shaded regions in the right panel show the regions where bottom pressure-stress curl is important in the meridional flow of the western boundary currents.[19]

that $\nabla\eta_B = -\nabla h$ where h is the fluid thickness. The second term on the right-hand side of (19.95) is the stress on the fluid due to a correlation between the pressure gradient and the topography at the ocean bottom — it is the bottom *form drag*, first encountered in Section 3.6.

Taking the curl of (19.95) gives

$$\beta\overline{v} = -\mathrm{curl}_z(\phi_B\nabla\eta_B) + \mathrm{curl}_z\overline{\boldsymbol{F}} = -J(\phi_B,\eta_B) + \mathrm{curl}_z\overline{\boldsymbol{F}}. \tag{19.96}$$

This equation holds for both a stratified and a homogeneous fluid. The first term on the right-hand side is the bottom pressure-stress curl, or the form-drag curl. (It is also sometimes informally referred to as the bottom pressure torque.)

Equation (19.96) is similar to (19.91), in that both arise from (19.95). To derive an equation with the same form as (19.91) but valid for a stratified fluid, we write the vertical integral of the pressure as

$$\int_{-h}^{0}\phi\,\mathrm{d}z = \int_{-h}^{0}\left[\mathrm{d}(\phi z) - z(\partial\phi/\partial z)\,\mathrm{d}z\right] = \int_{-h}^{0}\left[\mathrm{d}(\phi z) - zb\,\mathrm{d}z\right] = h\phi_B + \Gamma, \tag{19.97}$$

using hydrostatic balance, and where $\Gamma \equiv -\int_{-h}^{0} zb\,\mathrm{d}z$. Using (19.97) in (19.95) we obtain:

$$\boldsymbol{f}\times\overline{\boldsymbol{u}} = -h\nabla\phi_B + \nabla\Gamma + \overline{\boldsymbol{F}}. \tag{19.98}$$

The curl of this equation just gives back (19.96), but if we divide by h before taking the curl we obtain

$$J(\psi, f/h) + J(h^{-1},\Gamma) = \mathrm{curl}_z(\overline{\boldsymbol{F}}/h). \tag{19.99}$$

The second term in (19.99) is known as the JEBAR TERM — joint effect of baroclinicity and relief — and it couples the depth integrated flow with the baroclinic flow.[20] Thus, if the bottom is not flat, the Stommel–Munk models are not solutions for the vertically integrated flow. If the stratification vanishes (i.e., b is constant) then Γ is a function of h alone and $J(h^{-1},\Gamma) = 0$, and (19.99) reprises (19.91), given an appropriate choice of $\overline{\boldsymbol{F}}$.

Bottom pressure stress in a homogeneous gyre

For the remainder of this section we restrict attention to a homogeneous (i.e., unstratified) gyre. If there is no forcing or friction, then from (19.96) and (19.98) we see that the flow simultaneously satisfies

$$\beta v = -\nabla\phi_B \times \nabla\eta_B \equiv -J(\phi_b, \eta_B), \qquad \text{and} \qquad J(\psi, f/h) = 0. \tag{19.100a,b}$$

The right-hand side of (19.100a), the form-drag curl, is non-zero whenever the pressure gradient has a component parallel to the topographic contour (i.e., when the isobars are not aligned with the topographic contours). From (19.100b) we may conclude that if there *is* meridional flow in an unforced, inviscid fluid it must be along f/h contours, and this meridional flow may be thought of as being driven by the curl of the form drag. If the domain is flat-bottomed then the form drag is zero, and in that case all meridional flow is forced or viscous.

Real flows are both forced and viscous. Bottom pressure stresses may — and likely do — locally dominate viscous stresses. However, the bottom pressure-stress curl cannot balance the wind-stress curl when integrated over the whole domain, or indeed when integrated over an area bounded by a line of constant ϕ_B or constant η_B, because its integral over such an area vanishes and (19.91) cannot be balanced if $r = 0$. In the numerical simulations shown in Fig. 19.16, it is the bottom pressure-stress curl term that largely balances the poleward flow term (βv) in the vorticity equation in parts of the western boundary current, with friction acting in the opposite sense. That is, over some regions where the flow is crossing f/h contours we have the balance

$$[\beta v] \approx [\text{bottom pressure-stress curl}] - [\text{friction}], \tag{19.101}$$

where the terms in square brackets are positive, and friction is small. In contrast, in the flat-bottomed case in the western boundary layer we have the classical balance $[\beta v] \approx +[\text{friction}]$, with both terms positive.

Now consider the balance of momentum, integrated zonally across the domain. We write the vorticity equation (19.96) in the form

$$\nabla \cdot (f\overline{\boldsymbol{u}}) = -\text{curl}_z(\phi_B \nabla\eta_B) + \text{curl}_z \boldsymbol{\tau}_T - \text{curl}_z \boldsymbol{\tau}_B, \tag{19.102}$$

where $\boldsymbol{u} = (u, v)$, $\boldsymbol{\tau}_T$ is the wind stress at the top and $\boldsymbol{\tau}_B$ the frictional stress at the bottom. Integrate (19.102) over the area of a zonal strip bounded by two nearby lines of latitude, y_1 and y_2, and the coastlines at either end. The term on the left-hand side vanishes by mass conservation and using Stokes' theorem we obtain:

$$\int_{y_1} \phi_B \frac{\partial \eta_B}{\partial x}\, \mathrm{d}x - \int_{y_2} \phi_B \frac{\partial \eta_B}{\partial x}\, \mathrm{d}x = \int_{y_1} (\tau_T^x - \tau_F^x)\, \mathrm{d}x - \int_{y_2} (\tau_T^x - \tau_F^x)\, \mathrm{d}x. \tag{19.103}$$

If the topography is non-zero, there is nothing in this equation to prevent the wind stress being balanced by the form stress terms, with the friction being a negligible contribution. If, for example, friction were to be confined to the southwest corner, then bottom pressure stress is the proximate driver of fluid polewards in the western boundary current. This may hold only if the scale of the sloping sidewall is greater than the thickness of the Stommel layer; if the converse holds then the sidewalls appear to be essentially vertical to the flow. If the sidewalls are truly vertical, then the form stress is confined to delta-functions at the walls. Friction must then be important even in the zonal balance, because if we restrict the integral in (19.103) to a strip that does not quite reach the sidewalls, the left-hand side vanishes identically and the wind stress can only be balanced by friction.

To conclude this discussion, we note that the effects of topography are likely greater in homogeneous fluids than in stratified fluids, because the stratification will partially shield the wind-driven upper ocean from feeling the topography, but we leave the exploration of that topic for another day.

Notes

1 Paumanok is the Native American name for Long Island in New York state. Studying the natural world is a humbling experience, and Whitman's beautiful writing reflects my feelings. But to try to understand and convey that understanding is what we are drawn to do, is perhaps what we *have* to do.

2 Henry Stommel (1920–1992) was one of the most creative and influential physical oceanographers of the twentieth century. Spending most of his career at Woods Hole Institute of Oceanography, his enduring contributions include the first essentially correct theory of western intensification (and so of the Gulf Stream), some of the first models of abyssal flow and the thermohaline circulation (Chapter 21), and his foundational work on the thermocline. His *forté* was in constructing elegantly simple models of complex phenomena — often models that were physically realizable in the laboratory — while at the same time testing and encouraging others to test the models against observations. This chapter might have been entitled 'Variations on a theme of Stommel'.

3 Both Fig. 19.3 and Fig. 19.4 are 'state estimates' — outputs of a model constrained by or combined with observations in such a way as to produce an approximation of the ocean state, hopefully more accurate than either models or data can separately produce. An atmospheric 'reanalysis' is also a state estimate, but for historical reasons meteorologists use a non-standard terminology. Because of the dearth of data in the ocean compared to the atmosphere, oceanic state estimates are less accurate and more model dependant than their atmospheric counterparts.

4 Courtesy of R. Zhang. See also Zhang & Vallis (2007).

5 I'm grateful to P. Heimbach for this figure, obtained using the ECCO state estimation system.

6 The asymptotic solution to this boundary value problem was obtained by Wasow (1944), a few years prior to Stommel's work, and further investigated by Levinson (1950). However, it seems unlikely these two investigators were motivated by the oceanographic problem.

7 Harald Sverdrup (1888–1957) was a Norwegian meteorologist/oceanographer who is most famous for the balance that now bears his name, but he also played a leadership role in scientific policy and was the director of Scripps Institution of Oceanography from 1936–1948. The Sverdrup unit is also named for him. Originally defined as a measure of volume transport, with $1\,\text{Sv} \equiv 10^6\,\text{m}^3\,\text{s}^{-1}$, it is more generally thought of as a mass transport with $1\,\text{Sv} \equiv 10^9\,\text{kg}\,\text{s}^{-1}$, in which case it can also be used as a measure of transport in the atmosphere. The Hadley Cell, for example, has an average transport of about 100 Sv (Figs. 14.3 and 15.22).

8 Leetmaa *et al.* (1977) and Wunsch & Roemmich (1985) offer complementary views on the matter.

9 After Munk (1950). Many thanks to Manuel Lopez Mariscal of CICESE for a number of useful comments and corrections.

10 Hendershott (1987), Veronis (1966a).

11 Veronis (1966a,b) was one of the first to investigate nonlinear effects in wind-driven gyres. See also Fox-Kemper & Pedlosky (2004) and references therein.

12 Solutions kindly provided by B. Fox-Kemper.

13 After Charney (1955).

14 See also Greenspan (1962). Il'in & Kamenkovich (1964) and Ierley & Ruehr (1986) show numerically that the friction must be sufficiently strong for steady boundary-layer solutions to exist.

15 After Fofonoff (1954).

16 Hughes & de Cuevas (2001).

17 Welander (1968).

18 Figure kindly provided by Laura Jackson.

19 Adapted from Jackson *et al.* (2006).

20 Sarkisyan & Ivanov (1971).

Further Reading

Mainly theory and modelling

Abarbanel H. D. I. & Young, W. R., Eds., 1987. *General Circulation of the Ocean.*
Contains several useful review articles on the oceanic general circulation as it was then understood.

In increasing order of size, the following books cover a variety of topics in ocean circulation, all at about the graduate student level:

Samelson, R. M., 2011. *The Theory of Large-Scale Ocean Circulation.*

Dijkstra, H. A. 2008. *Dynamical Oceanography.*

Pedlosky, J., 1996. *Ocean Circulation Theory.*

Huang, R. X., 2010. *Oceean Circulation.*

Olbers, D., Willebrand, J. & Eden, C., 2012. *Ocean Dynamics.*
These last two books are both hefty treatises on the topic.

Treatments of El Niño are to be found in

Clarke, A. J., 2008. *An Introduction to the Dynamics of El Niño and the Southern Oscillation.*

Sarachik, E. and Cane, M., 2010. *The El Niño–Southern Oscillation Phenomenon.*

Description and observation

Talley, L. D., Pickard, G.L., W. J. Emery, W. J. & Swift, J. H. 2011. *Descriptive Physical Oceanography: An Introduction.*
This text gives a sense of the big picture, as well as being full of useful maps of ocean properties.

Wunsch, C. 2015. *Modern Observational Physical Oceanography.*
Shows how modern observing systems (floats, satellites, etc.) can be used alongside numerical models to provide a more complete view of the ocean.